Alzheimer Disease: The proposed role of tanycytes in the formation of tau tangles and amyloid beta plaques in human brain

Abbreviated title: Tanycyte-mediated waste removal from the brain

Ruth Fabian-Fine[1,2,*], Abigail G. Roman[1] and Adam L. Weaver[1]

[1]Department of Biology, Saint Michael's College, Colchester, VT 05439, USA

[2]Lead contact

*Correspondence: rfabianfine@smcvt.edu

Page Numbers: 45

Number of Figures: 1-11; tables: n/a; multimedia: n/a; 3D models: n/a

Number of Words: Abstract: 226, Introduction 638, Discussion 1697

Abbreviations

Aquaporin-4 aqua channel: AQP4

Alzheimer Disease (AD)

Amyloid beta (Aß)

Amyloid Precursor Protein (APP)

Glial Fibrillary Acid Protein (GFAP)

Immunoreactive (IR)

Presenilin1 (Pres1)

ABSTRACT

Currently, the causes for Alzheimer Disease (AD) are thought to lie in the formation of abnormal protein deposits including tau tangles and Amyloid ß (Aβ) plaques in the human cortex. These proteins are believed to accumulate in the brain due to impaired waste removal resulting in neurodegeneration. In an alternative hypothesis we have recently proposed the existence of an aquaporin4 aqua channel (AQP4)-expressing tanycyte-derived canal network that likely internalizes waste for removal from the brain. We propose that both Aβ and tau protein may play important structural roles in this canal system. In support of this hypothesis, we demonstrate the formation of waste-internalizing receptacles by AQP4-expressing myelinated tanycytes. Using RNA-scope *in situ* hybridization, immunohistochemistry, ultrastructural, and histological approaches, we demonstrate receptacle differentiation in tanycyte-derived 'swell-bodies.' We show that these receptacles are AQP4- and Aβ-immunoreactive and that related gene expression is observed in 'swell-bodies' where receptacle differentiation is observed. Through correlative light- and electron-microscopy in human and mouse brain, we demonstrate that both Aß and tau protein are associated with these waste-internalizing structures (Agre et al., 2002) and likely play important roles in the waste internalization process. Based on our findings, we postulate that the functional significance of Aß may be structural stabilization of waste-internalizing structures and canals to prevent their collapse during the uptake process. We propose that tau protein may govern the quantitatively appropriate release of waste-internalizing structures. We postulate that AD-related Aβ-plaques and tau tangles likely show hypertrophic pathologies of this glial-canal-system and associated waste-internalizing receptacles.

INTRODUCTION

Currently, the underlying causes for Alzheimer Disease (AD) are elusive and are thought to lie in the formation of abnormal intracellular deposits of hyperphosphorylated tau tangles and extracellular Amyloid ß (Aß) plaques throughout the human cortex. Due to this abnormal protein accumulation in AD-affected brain tissue, a prevalent causative hypothesis is failed waste removal

from the nervous system (Barichello de Quevedo et al., 2023; Buccellato et al., 2022; Iliff et al., 2012; Murdock et al., 2024). Currently, the way by which waste is cleared from the brain is poorly understood. Illiff et al. (2012) have proposed the existence of an aquaporin-4 aqua channel (AQP4)-mediated 'Glymphatic System.' Based on this postulation AQP4-expressing astrocytes are thought to flush cellular debris from the brain by means of a cytoplasmic convective flow of cerebrospinal fluid. Using two-photon microscopy and fluorescent tracers in mouse brain, the authors demonstrated the formation of a convective flow through the neuropil believed to flush cellular waste into peri-venous spaces for clearance from the brain (Iliff et al., 2012; Iliff and Nedergaard, 2013; Nedergaard, 2013; Nedergaard and Goldman, 2016). Interestingly, a significantly reduced flow of cerebrospinal fluid was observed in AQP4-null mice compared to wild-type mice (Mestre et al., 2018). This hypothesis however has been put into question predominantly regarding the proposed astrocyte-induced AQP4-mediated flow of brain fluids (Abbott et al., 2018; Buccellato et al., 2022). In an alternative model for waste removal from the brain, we have proposed that debris uptake may be mediated by a 'glial-canal system.' We postulate that this tanycyte-derived canal system is highly conserved between spider, rodent, and human brain and internalizes waste for removal from the brain parenchyma (Fabian-Fine et al., 2024). We propose that myelinated AQP4-expressing ependymal tanycytes form a syncytial network and contact neurons and glial cells for proposed waste removal via differentiating waste-internalizing receptacles. We have provided evidence that this canal system is structurally impaired in degenerating brain tissue. This structural impairment is manifested in the form of hypertrophic tanycyte swelling that leads to catastrophic obstruction, cytoplasmic depletion, and death of neurons. We have termed this macroglia-induced cell death 'gliaptosis' (Fabian-Fine et al., 2024).

To test our postulation that ependymal tanycytes internalize cellular matter, here we have conducted RNAscope gene expression together with immunohistochemical, histological, and ultrastructural studies. To support our postulations, we have furthermore conducted functional studies on living mouse brain to assess whether structures we have identified as waste-receptacles internalize fluorochromes as predicted. We provide evidence that these receptacles express the Aß-related genes for presenilin 1 (Pres1) and amyloid precursor protein (APP) and appear

immunolabeled for Aß. We furthermore demonstrate that these receptacles swell in AD-affected brain tissue and resemble Aß-plaques (Maarouf et al., 2008) in immunolabeled sections. Offering an alternative hypothesis we postulate that lining of waste-internalizing receptacles and canals by structurally stable Aß aggregates (Tycko, 2015) may provide structural stabilization of these waste-internalizing structures to prevent their collapse during AQP4-mediated waste intake.

MATERIALS & METHODS

EXPERIMENTAL MODELS AND STUDY PARTICIPANT DETAILS

Mouse brain tissue

The mouse brain originated from adult (6- to 15-month-old) female wildtype strain is Cdh5-GCaMP8 mice. For ethical reasons and to avoid unnecessary animal sacrifices, the brains used in this study were obtained from surplus tissue. The tissue was obtained freshly upon dissection of the animals and processed as described below. IACUC approval was granted under PROTO202200018 (University of Vermont) and IACUC-2024-001 Fabian-Fine (Saint Michael's College).

Human brain tissue

The human brain tissue used for our investigations originated from tissue used in a previous study (Fabian-Fine et al., 2024). As stated in this publication, the tissue was fully consented including 'consent for research' from next of kin in compliance with Vermont and institutional laws (Health and Human services regulation 45 CFR 46.102 e). In brief: The tissue originated from four Caucasian decedents. The autopsy examination was carried out by Dr. John DeWitt at the University of Vermont Medical Center in the context of a previously published study (Fabian-Fine et al., 2024). The tissue samples of AD-decedents were consistent with high (86-year-old female) and intermediate (86-year-old male) burdens of ADNC (for more detail, see Fabian-Fine et al 2024).

Experimental Design and Statistical Analysis

Uptake experiments on living mouse brain

Three mice from which the surplus brain tissue was obtained were euthanized with Euthasol (Virbac) by a licensed technician. The brains were immediately removed from the cranium and transferred into mouse culture medium DMEM (VWR Cat #45000-312) containing 4.5 g/L glucose, L-glutamine, 10% Fetal Bovine Serum and 1% Penicillin/Streptomycin at 37 °C to maintain temperature appropriate enzymatic activity. The two brain hemispheres were separated, and each hemisphere was sliced into three equal coronal sections along the anterior-posterior axis. The sections from the right hemisphere (controls) were kept in culture medium, whereas the left hemisphere sections (experimental) were kept in culture medium to which we added Cy3-coupled goat-anti rabbit secondary antibody (Jackson ImmunoResearch # 111 -165-003). After 30 min, both control and experimental brain sections were fixed with freshly made 4% paraformaldehyde (4% PFA) overnight at 6 °C. The preparations were embedded in 4% agarose (Sigma 9539) and sectioned into 70-µm vibratome sections using a Leica Vibratome 1000S. The sections were washed in PBS and mounted on glass slides using Mowiol (Sigma 81381). The sections of both control and experimental preparations were imaged with identical settings using a Zeiss Axio-Imager confocal microscope with ZEN-Blue software. To test that the internalized fluorochrome detected in ependymal cells of the experimental preparations indeed originate from the Cy3-coupled goat antibody, we utilized a secondary Alexa 488-coupled donkey anti-goat antibody (Jackson ImmunoResearch # 705-545-003). For this purpose, additional sections were cut and washed in 0.1 M phosphate-buffered saline pH 7.4 (PBS). Unspecific binding sites were blocked with blocking medium containing 0.25% Bovine Serum Albumin (Sigma A4503) and 5% Normal goat serum (Sigma G9023) in 1% Triton-X/PBS for 20 min prior to incubation with the donkey anti-goat antibody (1:600 overnight at 6 °C). Subsequently, the preparations were washed in PBS (2x5 min), stained with Hoechst Blue nuclear stain (1:3000; 15 min), washed in PBS 5x10 min, and mounted on glass slides using Mowiol prior to examination with the Zeiss confocal microscope.

Image and Statistical Analysis

Confocal images were exported from the Zeiss ZEN-Blue program using the “Original Data” setting and analyzed in CellProfiler 4.2.8 for all measurements (Stirling et al., 2021). Briefly, Cy3 stained objects were identified [Three-class Otsu thresholding; middle class: background] that were brighter than the background and had a diameter between 5 and 60 µm. Object size/shape and intensity were measured. In some cases, full captured images had their exposure minimally modified to enhance contrast or brightness identically for figures, but not for the analysis.

An unpaired, two-tailed Student’s t-test with Welch’s correction was used to perform comparisons of the Log_{10} mean object intensities across control (0 µM) and TGN-020 AQP4-blocked (60 µM; Sigma SML0136) conditions. All statistical parameters and results are reported in the relevant figure legend. To the best of our knowledge, all assumptions of this test were met. Statistics were calculated and graphs were created using Prism 10.4.1 (GraphPad Software).

Tissue Processing for semi- and ultrathin sectioning

Hippocampal tissue samples (~50 mm thick) were immersed in freshly prepared ice cold 4% paraformaldehyde (EMS 15710) and 2.5% glutaraldehyde (EMS 16019) in phosphate buffered saline (pH 7.4, 0.1 M; PBS) and fixed for at least 48 hours in the refrigerator. The preparations were embedded in 4% agarose and sectioned, postfixed in 1% osmium tetroxide, dehydrated in a graded series of ethanol, and embedded into Araldite as described previously (Fabian-Fine et al. 2024). Using a Diatome Histo-knife with 8 mm blade ultrathin sections (50-60 nm) were cut with a Leica Ultracut E.

The sections were stretched with chloroform (Electron Microscopic Sciences 12540) by gently waving a chloroform-soaked wooden toothpick over the sections without touching them until they were sufficiently stretched. The sections were collected on pioloform-coated single-slot copper grids (EMS G2010CU) using #5 Dumont forceps and an eyelash that was mounted to a wooden toothpick using hot bee’s wax. Grids were contrasted with aqueous 1.5% uranyl acetate (6 min) and Reynold’s lead citrate (6 min) according to standard electron microscopic methods. The

examination was conducted using a JOEL 1400 electron microscope with digital image acquisition operated at 80 kV.

Light Microscopic Immunohistochemistry

Human hippocampal tissue utilized for light-microscopic immunolabeling was fixed in freshly prepared, ice-cold 4% paraformaldehyde for a minimum of 48 h at 6 °C. The tissue was embedded in 4% Agarose, sectioned into 70-µm vibratome sections using a Leica Vibratome 1000S. The sections were washed in PBS 4x5 min and unspecific binding sites were blocked with blocking medium containing 0.25% Bovine Serum Albumin (Sigma A4503) and 5% Normal goat serum (Sigma G9023) in 1% Triton-X/PBS for 20 min. The sections were incubated overnight at 6 °C within the respective primary antibody solutions (rabbit anti-aquaporin-4 antiserum BiCell 20104, rat anti-Caspase2 BiCell 10302, Anti-Pres1; Sigma Aldrich ZRB1614, Anti-APP-C99; Sigma Aldrich MABN380, mouse anti-α-tubulin 12G10, DSHB, IOWA, and anti-Myelin 6-4H2 DSHB, IOWA) at dilutions of 1:100. Prior to incubation with the secondary antibodies, preparations were washed thoroughly in PBS (5x10 min), incubated in blocking medium as described above, and incubated with either secondary Cy3 goat anti-rabbit (Jackson ImmunoResearch Laboratories 111-165-003), Cy3 goat anti-mouse (Jackson ImmunoResearch # 115-165-148), and Cy3 goat-anti rat (Jackson ImmunoResearch # 112-165-003) at dilutions of 1:600 in PBS containing 10% blocking medium overnight at 6 °C. Subsequently, the sections were rinsed in PBS (3x2 min). For the nuclear stain, we utilized Hoechst Blue (Sigma Aldrich 94403-1ML) at a dilution of 1:3000 in PBS for 20 min. After washing in PBS (5x10 min), the sections were mounted on glass slides using Mowiol (Sigma 81381). To avoid bleaching of the fluorochromes, the mounting was conducted with minimum illumination.

Immunoperoxidase stain for Aβ and Tau protein: Immunolabeling for both A*β* and Tau 8 were conducted on paraffin embedded 8-µm sections as previously described (Fabian-Fine et al. 2024)

Luxol H&E staining of Autopsy Tissue: The histological staining methods were carried out as previously described (Fabian-Fine et al. 2024).

RNA-scope In Situ RNA Hybridization: The RNA-scope methods to detect APP, AQP4 and Pres1-RNA expression were carried out as described previously (Fabian-Fine et al. 2024).

Light Microscopic Image Acquisition: Histological brain sections were examined and captured using an Olympus light microscope with digital image acquisition. Figures were created using Adobe Photoshop and Illustrator.

RNAscope control experiments: The RNA integrity in the human brain tissue was tested in all samples. We used *in situ* hybridization for the human 'housekeeping' gene peptidylpropyl isomerase B, which is expressed at low levels. The observed expression of this gene thus demonstrated sufficient preservation of RNA in our tested brain samples. For negative controls, the bacterial gene dapB was utilized. The absence of fluorescent signals in the negative control supports the specificity of our detected AQP4, Pres1, GFAP and APP-RNA expression signals.

Immunohistochemistry negative controls: The antibodies utilized here have been well-established in the human brain. We have routinely carried out negative controls in which the primary antibodies were omitted to exclude that the observed strong fluorescence may be attributed to autofluorescence in the tissue.

RESULTS

Aquaporin-4 and myelin double-labeled ependymal tanycytes form 'swell-bodies'

In both mouse and human hippocampus ependymal tanycytes whose somata reside in the temporal horn of the lateral ventricles form an extensive network of long, myelinated, slender processes (indicated by Luxol-blue stain in Figure 1A, B) that emanate from the alveus and project into the hippocampal stratum pyramidale (Figure 1E). In both human and mouse hippocampus, the AQP4-immunolabeled nature of these myelinated, slender processes is apparent (Figure 1C, D, J-K). It is likely this AQP4-expressing nature of tanycytes that leads to water influx into these glial cells that explains different swelling patterns in individual tanycyte processes (Figure 1H, see

discussion). Both Luxol-blue stain in human hippocampus (Figure 1H) and double immunolabeling for AQP4 and myelin in mouse hippocampus (Figure 1I-K) show myelin-labeled circular structures that line the inside of these glial processes reminiscent of stabilizing cartilaginous rings in trachea (Figure 1 H-K; see discussion).

Another organelle type that is formed along AQP4-expressing myelinated tanycyte processes are circular electron lucent 'swell-bodies.' These organelles are clearly visible in Luxol H&E-stained human hippocampus and AQP4/myelin immunolabeled mouse hippocampus (Figures 1; 2A-D). Each swell body contains between one and six circular organelles that stain for nuclear stain and appear physically associated with myelinated tanycyte processes (Figure 1O-T). Unlike typical cell nuclei, these organelles give rise to receptacles that internalize electron-dense waste (Figures 1Q, S, T; 2A-D; see also below). Due to three distinct characteristics that distinguish these nucleus-like structures from conventional cell nuclei, we will refer to these nucleus-like structures as 'tanysomes.'

Tanysome versus conventional cell nucleus

Despite the positive nuclear stain, three main features distinguish tanysomes from conventional nuclei found in cell bodies. These features can be observed in both non-AD affected and AD-affected tissue and include: *(i)* the emergence of the aforementioned varicose waste-receptacles from these organelles (Figure 1 S, T; see more detail below), *(ii)* our observation that these nucleus-like organelles are physically connected with myelinated tanycyte processes (Figures 1, 2), and *(iii)* the emergence of swelling toroid-shaped structures from tanysomes (Figures 1R; 2). These membranous ring structures swell to widely varying diameters of >20 μm. Interestingly, they stain for anti-phosphorylated tau protein, anti-α-tubulin, anti-Aβ, anti-AQP4, anti-myelin and Luxol-blue H&E stain (Figure 2). Like tanysomes from which toroids emerge, the latter often stain for nuclear stain and give rise to varicose receptacles (Figure 2M).

Tanysomes and tanycyte processes give rise to waste-internalizing myelin-derived waste receptacles

The lumina of swell-bodies that are void of receptacles appear clear at the light microscopic level in Luxol H&E-stained preparations and electron lucent at the electron microscopic level (Figure 1O) unlike the structured cytoplasmic appearance in neuronal and glial cell somata (Figure 1O). In other swell-bodies tanysome derived membranous structures give rise to interconnected membrane networks that predominantly originate from tanysomes and form swelling donut-shaped structures (Figure 2 H, I; in the following referred to as 'toroids') and circular receptacles (Figure 2D; for more detail see below). Electron-microscopic examination reveals the formation of receptacles that emanate from tanysomes (Figure 1Q, R). The appearance and diameters of these receptacles vary widely from electron-lucent with diameters of ~20 nm to electron-dense with diameters of up to 1 μm (Figure 1Q, T, for more detail see below). The blue coloration of larger receptacles in Luxol H&E-stained human brain preparations is suggestive of their myelinated nature (Figure 2C, D; more detail is provided in Figure 6).

Tanycyte-derived receptacles project into neuronal somata

Immunolabeling demonstrates the AQP4-IR nature of waste receptacles that emanate from tanysomes (Figure 3A). Investigation of Luxol H&E-stained brain sections show strands of Luxol-blue stained waste receptacles that emanate from tanysomes project into neuronal somata in both AD-affected and AD-unaffected human hippocampus (Figure 3C-G). Please note the close association of the swell body with the neuronal somata in non-AD affected tissue, which leads to a convex indentation consistent with hydrostatic pressure exerted on the soma (Figure 3G). In AD-affected brain tissue, the receptacles appear hypertrophic compared to non-AD-affected tissue (Figure 3). These findings are consistent with ultrastructural observations that show (*i*) numerous waste receptacles within neuronal somata and their association with electron-dense cellular waste (Figure 3H), and (*ii*) the dense obstruction of neuronal somata with waste receptacles in AD-affected human brain tissue that is often associated with cytoplasmic depletion (Figure 3H, J). In contrast, neurons in non-AD affected human hippocampus show small numbers of waste receptacles and intact cytoplasmic structure (Figure 3I).

Functional evidence for AQP4-mediated waste intake into ependymal tanycytes

To further test our hypothesis that the observed electron-dense material observed in tanycyte-derived waste receptacles is internalized cellular matter, we have investigated fluorochrome uptake by ependymal glial cells in living mouse hippocampus. Within 30 min of exposure to culture medium to which Cy3-conjugated goat anti-rabbit antibody was added, the above-described tanycytes and associated ring structures with emanating receptacles appear brightly fluorescent (Figure 4). In contrast, control preparations that were void of the fluorochrome lacked fluorescence. These findings are consistent with our hypothesis that the fluorochrome may be internalized by these ependymal tanycytes (Figure 4). The ventricular lining showed a fluorescing, interconnected network of tanycyte processes and canals each containing two small-diameter fluorescent channels within their lumina (Figure 4D insets). These canals project into the adjacent ventricular lumen (Figure 4E, bottom inset). To confirm that the internalized fluorochromes are indeed the Cy3 goat-anti rabbit antibodies, we have immunolabeled these brains with an Alexa 488-coupled donkey-anti goat antibody. The double-labeled nature of fluorescent structures (Figure 4A-C) aligns with our postulation that the fluorescence observed within ependymal tanycytes is indeed due to the uptake of the Cy3 conjugated antibody. Interestingly, tanycytes that border directly onto the ventricle form apical canals that project into the ventricular space (Figure 4A). To investigate our hypothesis that the observed internalization of the applied fluorochrome is AQP4-mediated, we have conducted additional experiments in which we have separated and sectioned the two hemispheres of mouse brains. The brain sections of one hemisphere served as control and were kept in culture medium only, the experimental sections from the second hemisphere were immersed in culture medium that contained 60 μM of the selective AQP4-blocker TGN-020. Both hemispheres were then exposed to the Cy3-conjugated antibody. Analysis of these preparations revealed a significantly reduced fluorescent signal within TGN-020-exposed brain cells compared to the controls in comparable brain areas (Figure 4E-F). Comparisons of Log_{10} mean cellular object pixel intensities demonstrate significantly higher pixel intensity in control (0 μM; -1.888) compared to AQP4-blocked (60 μM TGN-020; -2.278) conditions (Figure 4G). Fluorescence was absent in

nearby neurons. We postulate that the observed fluorescence in tanycytes may originate from tanycyte-derived, strongly fluorescent receptacles that internalized waste from extracellular spaces. As demonstrated in Figure 4I, the fluorescent structures strongly resemble in shape and size the receptacles visualized with Luxol Blue H&E stain, Aβ, and AQP4/myelin immunolabeling in both human and mouse hippocampus.

Waste-receptacle associated gene expression in tanysomes

Based on our findings, we postulate that AQP4 and Aβ may be two important functional and structural proteins that are expressed by tanysomes in swell bodies where receptacle formation takes place. We postulate that AQP4 may mediate a convective bulk flow toward the receptacles to flush cellular debris toward these proposed waste-internalizing structures. We further postulate that the role of Aβ may be the structural stabilization of these receptacles to prevent their collapse during the uptake process. We hypothesize that glial fibrillary acid protein (GFAP) may play an important role in the formation of waste receptacles. Since transport of large amounts of structural proteins through narrow tanycyte processes would likely lead to their obstruction we investigated whether these proteins may be expressed by tanysomes in swell bodies where receptacle formation is observed. To evaluate this hypothesis, we have employed RNA-scope gene expression testing AQP4-, GFAP-, Pres1-, and APP-RNA expression in swell-bodies and associated tanysomes throughout human hippocampus. We have furthermore conducted immunohistochemical labeling for Aβ, APP, Pres1 and AQP4 to test if the expressed proteins are detected along waste receptacles. As demonstrated in Figures 5 and 6 both approaches show strong gene expression for all tested probes in swell-bodies. Size, appearance, and location of the structures that show both gene expression and immunolabeling are consistent with tanysomes and their associated toroids and receptacles described above (Figures 2, 5, 6). Interestingly, the distribution of GFAP-RNA appeared less restricted to swell-bodies compared to AQP4-, APP- and Pres1-RNA, which may indicate the transport of GFAP-RNA within tanycyte processes. Immunolabeling for APP, Pres1, AQP4 and Aβ is present along waste receptacles consistent with

the gene expression patterns. Interestingly, the comparatively low level of Pres1-RNA expression at tanysome-derived receptacles (Figure 6 G, M) compared to the stronger APP-RNA signal (Figure 6H, N) is consistent with the signal strengths observed in Pres1/APP immunolabeled preparations (Figure 6V Pres1; 6X APP). Neuronal cell bodies and somata that are consistent with the appearance of astrocytes appeared consistently unstained (Figure 5). Not all tanysomes showed gene expression, which is consistent with our observations in Aβ-immunolabeled preparations (Figure 7E) and may be due to various stages of differentiation and maturation. Closer investigation of Aβ-immunolabeled swell-bodies shows the emergence of membranous receptacles from strongly Aβ-immunoreactive toroids (Figure 6Q, R). These observations are consistent with ultrastructural investigation of swell bodies that show the emergence of receptacles from myelinated cell processes (Figures 6 S, T, U Ai; 7P; 8D, E). The electron-dense appearance of some of these receptacles at the ultrastructural level is consistent with our postulation of waste uptake. Our hypothesis that this waste may be enzymatically catabolized by caspases is supported by the homogenous appearance of this waste and anti-caspase2 and 3 immunolabeling both of which show strong immunolabeling in receptacle-containing swell bodies (Figure 6Z, Ai).

Amyloid β plaques in AD-affected human hippocampus are consistent with hypertrophic tanysome-derived waste receptacles

To test our hypothesis that Aβ-plaques in AD-affected hippocampus may originate from hypertrophic waste receptacles that emanate from swell-bodies we have investigated anatomical characteristics of Aβ-immunolabeling in human hippocampus.

In AD-unaffected brain tissue modest Aβ-immunolabeling along tanysome-derived waste receptacles was observed. Consistent with our Luxol H&E-stained preparations, immunolabeled receptacles were frequently observed within swell-bodies and projecting into neuronal somata (Figure 7A, D). Similarly, only weak anti-tau staining was observed around waste receptacles in swell-bodies (Figure 7B). In contrast, immunolabeling of AD-affected hippocampus showed strong immunolabeling for both proteins. Similar observations were made in AD-affected brain tissue

stained for anti-α-tubulin (see discussion). Compared with non-AD affected brain tissue, the labeled receptacles appeared denser and more hypertrophic in AD-affected tissue giving them the typical appearance of Aβ-plaques (Figure 7). Although the strong Aβ labeling of hypertrophy toroids and receptacles observed in AD-affected tissue makes recognition of labeled structures difficult, their association with tanysomes and swell-bodies is clearly visible (Figure 7 I, J). We have provided complementary histological and ultrastructural images together with schematic drawings to explain the structures that stain for tau-, Aβ-, and α-tubulin proteins (Figure 8). As described earlier, tanysomes in swell-bodies give rise to myelinated receptacles (Figures 2, 7). These findings are consistent with our ultrastructural investigations that show waste receptacles emanating from myelinated cell profiles (Figures 6, 7, 8). Figure 8 D, E demonstrates that strands of receptacles emerge from clearly visible pores in myelinated processes. The GFAP-like fibrillary structures that emerge from the myelinated processes differentiate into numerous bulging waste receptacles with increasing distance from the myelinated process (Figure 8 D, E). The distal ends of these receptacle strands merge into distal ring structures that form within this intricate membrane network and can be seen pulling out of neuronal somata and swell-bodies (Figure 8A). Strong anti-tau immunolabeling and fibrillary structures commonly described as 'intracellular tau tangles' are formed by these swelling myelin-derived circular structures that unravel and form numerous strands of waste receptacles (Figure 8H, I, J). Please note, the electron-dense appearance of the depicted waste receptacles strands in Figure 8D, E, compared with those shown in Figure 6T that are in the forming process. These observations are suggestive of waste internalization within fully formed receptacles depicted in Figure 8. Systematic analysis of anti-tau immunolabeled AD-affected hippocampus shows that anti-tau immunoreactivity is strongest within neuronal somata (Figure 8B). However anti-tau immunoreactive tanysome-associated toroids and receptacles can be observed throughout the hippocampal formation (Figures 8, 9). Please note the 'unraveling' of numerous receptacle strands from anti-tau-stained toroids (Figures 7L, M, Q; 8H, I) in AD-affected tissue. Higher zoom of waste receptacles in Aβ-immunolabeled human hippocampus reveals an intricate network of fine canal structures that: (*i*) connect the centrally located toroid-shaped ring structure with emanating waste receptacles, and (*ii*) project from waste receptacles into the surrounding

space (Figure 8K). We propose that these structures are part of this waste-internalizing system, and that Aβ may play an important role in the structural stabilization of these canals to prevent their collapse during waste intake (see discussion).

Tanycyte-associated hypertrophic pathologies of human hippocampus in AD-affected brain tissue

Comparisons between AD-unaffected and AD-affected brain tissue demonstrate that structural abnormalities in the latter are consistently associated with swelling tanycyte processes. Structural differences between tanycyte processes in the alveus are particularly apparent in anti-tau labeled and Luxol H&E-stained preparations (Figure 9A-F). In non-AD affected tissue tanycytes and swell-bodies with associated tanysomes often project in parallel fashion. Although tanysomes form receptacles, they are only weakly stained for tau-protein (Figure 9B, C). In contrast, AD-affected tanycytes appear spongiform, due to the formation of numerous circular structures and bulging waste receptacles that emanate from tanysomes (Figure 9D-F, M, N). The heavily myelinated and swelling nature of these tanycyte-derived ring structures is evident in Luxol H&E-stained brain sections (Figure 9D, inset, M). The comparatively strong Tau-immunolabelling in AD-affected brain tissue is predominantly associated with tanysomes, swelling toroids and associated receptacles (Figure 9D-E, O, P). Similar hypertrophic abnormalities can be observed in swell-bodies (Figure 9I-L), neurons (Figure 9G, H) and tanycyte processes (Figure 9M, N, O, R). We repeatedly observed tanycyte swelling associated with bulging receptacles in the vicinity of brown deposits along tanycytes, the appearance of which is consistent with cellular waste (Figure 9J).

Based on the findings presented here, we propose that ependymal tanycytes give rise to a dense network of cell processes that form swell-bodies (Figure 10). Swell bodies contain tanycyte-derived AQP4-, GFAP-, Pres1-, and APP-expressing tanysomes from which a membranous network of toroids and receptacles emanate. Whereas some receptacles project into cell somata, others project into extracellular spaces. Based on our functional experiments, we postulate that swell-bodies, and waste receptacles form functional units that are part of a vast glial cell network which internalizes and removes intra- and extracellular waste from the brain in an AQP4-dependent manner (Figure 10). We postulate that waste is flushed toward the receptacles through the

formation of an AQP4-mediated convective flow toward the receptacles (Figure 11). We propose that Caspases 2 and 3 may play an important role in waste catabolism. We postulate that hypertrophic swelling of this tanycyte-derived waste canal system leads to obstruction and depletion of neuronal somata culminating in gliaptosis (macroglia-induced cell death).

DISCUSSION

Our findings support previous findings that myelinated ependymal tanycytes form waste-internalizing receptacles (Fabian-Fine et al., 2024). We describe specialized waste-internalizing organelles that consist of: (*i*) swell-bodies, (*ii*) nucleus-like tanysomes, and (*iii*) tanysome-derived toroids and waste receptacles that are structurally stabilized by Aβ. We postulate that these organelles play important roles in waste clearance from the hippocampal formation.

Anatomical and functional significance of swell-bodies and waste receptacles

Our light- and electron-microscopic findings shown here strongly support the formation of waste internalizing receptacles. We propose that swell-bodies and associated tanysomes form discrete compartments that govern the differentiation of AQP4-, Caspase 2 and 3, and Aβ-expressing waste receptacles. These findings are consistent with previously reported findings where we have shown the Pres1-immunoreactivity along tanycyte processes that project into neuronal somata where they express APP (Fabian-Fine et al., 2024). The expression of these proteins in swell-bodies that are distant from the associated ependymal tanycyte somata are likely important to ensure rapid and consistent availability of waste internalizing structures throughout the stratum pyramidale. Our observation that not all swell bodies show gene expression suggests that swell bodies may be highly dynamic structures that are continuously formed. This proposed mechanism poses the question how gene expression and receptacle formation within swell-bodies may be governed. Interestingly, in developmental processes gene expression is predominantly governed by localized paracrine factors, calcium signaling, and concentration gradients. It is thus feasible that differences in extracellular signaling factors and swelling patterns may promote or inhibit the differentiation of

receptacles. In this context, increased swelling that results in changing concentration gradients may favor receptacle differentiation. We stress to investigate previous observations by Jo et al. regarding the synergistic regulation of swelling patterns in retinal glial cells by AQP4 and the transient receptor potential isoform 4 (TRPV4) channel (Jo et al., 2015; Liedtke and Friedman, 2003). It is feasible that this swelling-sensitive calcium-permeable cation channel triggers gene expression in swell-bodies that leads to the differentiation of waste receptacles whose slender processes may be stabilized by Aβ to prevent collapse during waste intake. This hypothesis would be consistent with the excessive formation of swelling Aβ-immunoreactive waste receptacles in AD-affected brains shown here.

Fluorochrome uptake by tanycytes

While we acknowledge the limitations of the fluorochrome internalization in living mouse brain, we have included these experiments to further support our histological and ultrastructural findings. The observed fluorescence in ependymal tanycytes is consistent with our predictions of AQP4-mediated waste internalization by these cells. The fluorescent structures observed in single optical confocal sections are consistent with (i) shape, (ii) size and (iii) location of receptacles observed in immunohistochemical and histological human brain sections. We do not dispute that future experiments are required and should include the work with organotypic brain cultures and fluoro-nanogold that will enable us to conduct correlative light and ultrastructural investigations. We propose to further test the role of other brain-expressed AQP-subunits including AQP1 and 9 (Badaut et al., 2014).

Proposed functions of tau protein and Aβ

Amyloid β: In both AD-affected and -unaffected hippocampus waste receptacles are *Aβ-immunoreactive*. The structural clarity of Aβ-lined waste receptacles is inconsistent with the currently proposed random accumulation of misfolded Aβ-aggregates (Gupta and Goyal, 2016). We postulate that receptacles are important for waste removal from the brain in an AQP4-mediated

manner. One *key requirement* for such a system is the structural stability of the waste-internalizing components to prevent their collapse during waste intake. One comparable example is tracheal cartilaginous rings that prevent tracheal collapse during respiration. We postulate that Aβ provides similar structural stability to waste-internalizing structures. Investigations regarding the structural architecture of Aβ have revealed the formation of very stable cylindrical amyloid fibrils, consistent with Aβ-immunoreactive fibrils at waste receptacles shown here (Tycko, 2015).

Tau protein: Besides the structural stability of waste-internalizing structures, a second requirement for the proposed waste removal system is the appropriate formation of waste-internalizing receptacles. Too few receptacles may not sufficiently remove cellular waste, whereas too many receptacles may lead to excessive depletion and cell damage as demonstrated in spider CNS (Fabian-Fine et al., 2024). Our observations of anti-tau labeling demonstrate that the formation of characteristic 'tau tangles' is consistently associated with the 'unraveling' of myelinated tanycyte processes that give rise to both intraneuronal and extracellular strands of waste receptacles. Interestingly, previous observations in degenerating spider brain demonstrated that individual myelin sheaths are anchored to microtubules in the form of 'microtubule-associated-breaking points' (Fabian-Fine et al., 2024). The proposed functional significance of these structures is the regulated release and gradual availability of myelin-derived waste-internalizing glial canals. We propose to investigate whether microtubules may have a similar regulatory function regarding the release of waste receptacles. It is feasible that the receptacle release may be governed by tau protein through regulation of the dynamic instability of microtubules. Such processes would be uniquely suitable for the 'on-demand' release of waste receptacles throughout the brain. This would also explain our observations of weak anti-tau labeling in the vicinity of waste receptacles in non-AD-affected brain tissue. Here, we would expect the physiologically appropriate release of waste receptacles. It is feasible that stabilizing functions of microtubules fail in AD due to high intracellular pressure in swelling tanycytes resulting in unraveling of myelinated tanycyte profiles that leads to excessive obstruction and depletion of neuronal somata shown here. The strong co-localization of tanycyte-derived waste receptacles with α-tubulin shown here supports this hypothesis. We

propose that such processes take place both in intra- and extracellular places. As demonstrated here, extracellular tanycyte-derived myelin ring structures that unravel are generally less conspicuous compared to their intraneuronal counterparts. It is likely for this reason that tau-tangles have been predominantly associated with intraneuronal locations (Trejo-Lopez et al., 2022).

Proposed role of GFAP

The role of GFAP in the formation of waste-internalizing canal structures and their interactions with microtubules is unclear. Three observations lead us to suggest that GFAP may play an important role in waste receptacle formation. (*i*) The strong GFAP gene expression in tanysomes and derived waste receptacles. (*ii*) The strong resemblance of the canal structures that emanate from pores in myelin-rings with the described ultrastructural appearance of GFAP (Nahirney and Tremblay, 2021). (*iii*) The abundance of GFAP-RNA in tanycyte processes throughout the hippocampal formation. We propose that GFAP may be a key structural protein for the formation of waste-internalizing receptacles.

Tanycyte hypertrophy

We propose that tanycyte-related swelling may be caused by ingestion of toxins that likely accumulate in tanycytes and may damage these waste-internalizing glial cells. Consistent with this hypothesis are reported case studies showing onset of chemotherapy-induced leukoencephalopathy, a brain condition associated with spongiform abnormalities and loss of myelin (Moore-Maxwell et al., 2004).

Due to the severe hypertrophy in tanycytes that contain waste obstructions we postulate that swelling may be due to the blockage of drainage canals by insufficiently catabolized waste. This may explain the high incidence of AD-patients impacted by infections (Bruno et al., 2023; Mancuso et al., 2019; Sait et al., 2021; Sigurdson et al., 2019). The chitin-based structural architecture of fungal pathogens may not be sufficiently catabolized by endogenous enzymes prior to uptake into narrow tanycyte processes. Evidence in support of this hypothesis is demonstrated in a study by Alfonso et al. that illustrates the presence of fungal proteins in tanycyte-like processes, see Figures

3 and 4 in (Alonso et al., 2015). This would also explain the higher prevalence of AD among women compared to men (Niu et al., 2017) as women are more prone to fungal infections.

Identification of astrocytes, oligodendrocytes, and axonal processes

Our RNA-scope experiments show that tanycyte-derived swell bodies that contain tanysomes and waste receptacles show gene expression for GFAP and AQP4. The appearance of these organelles is markedly different from characteristically mononucleated astrocytes that show structured cytoplasmic content. Interestingly, immunohistochemical investigations of human cortical structures identified as astrocytes depict structures that strongly resemble tanysomes and associated waste receptacles shown here, see Figure 1 (Forrest et al., 2023). We have observed similar inconsistencies regarding myelination and oligodendrocytes. As demonstrated here at the electron-microscopic level, myelin-derived strands of waste receptacles protrude from clearly myelinated cell profiles. Until recently, myelination has been associated exclusively with oligodendrocytes and axonal processes for the purpose of axonal insulation. It has also not escaped our attention that the structures we describe as swell-bodies are often referred to as oligodendrocyte somata or satellite cells whose electron-lucent 'fried-egg' appearance is attributed to fixation artifacts (Garman, 2011; Komori, 2017). We clearly demonstrate, at both light and electron microscopic levels, that swell bodies do not have a cytoplasm or organelles that are observed in adjacent neuronal and glial somata. We show however, that swell-bodies are AQP4 positive and contain waste-internalizing, electron dense receptacles that emanate from tanycyte-associated tanysomes. Our findings that these receptacles express both AQP4-RNA and GFAP-RNA further supports our hypothesis that these structures may indeed represent tanycyte-derived organelles. Further evidence is provided by our observations that tanycytes in the ependymal lining show identical expression patterns. In contrast, oligodendrocytes are reportedly AQP4-negative (Amiry-Moghaddam and Ottersen, 2003).

Fixation artifact versus functional structure

Imperfections in myelin are often attributed to fixation artifacts (Möbius et al., 2010; Möbius et al., 2016). However, several arguments indicate that myelin-protrusions are likely of functional significance. (*i*) Our observations of fluorochrome-internalizing receptacles in living mouse brain show that swelling protrusions exist in living fluorochrome internalizing brain tissue. (*ii*) Myelinated tanycyte processes are consistently more spongiform in degenerating brain tissue, including perfused spider and rodent brain (Fabian-Fine et al., 2023; Fabian-Fine et al., 2024). (*iii*) Aquaporin-mediated swelling of cells is not novel. This phenomenon was demonstrated in frog oocytes that received AQP1-water channel cRNA. The resulting water influx into the eggs induced swelling and bursting of the cells (Preston et al., 1992). Characteristic swell patterns of AQP-expressing cells are utilized to develop AQP-agonists and antagonists (Wang et al., 2023). (*iv*) We demonstrate the structural integrity of waste receptacle strands that emanate from well-preserved pores in myelinated human tanycytes consistent with our light-microscopic findings. (*v*) Spongiform pathologies of brain tissue in neurodegeneration have been widely accepted as a hallmark in neurodegenerative diseases including both Creutzfeldt-Jakob Disease and AD (Sigurdson et al., 2019; Smith et al., 1987; Whatley et al., 2008).

Prevention of ion leakage from receptacle-containing neurons

Neuronal signal transduction depends on the integrity of electrochemical ion gradients. Holes in the neuronal membrane are therefore detrimental to signal transduction. Interestingly, swell-bodies in non-AD affected brain tissue form visibly concave indentations in the neuronal somata likely due to hydrostatic pressure associated with fluid-filled swell-bodies. The resulting tight association between the neuronal and swell-body membranes may thus effectively seal the point of tanycyte entry into neurons and prevent leakage flow.

Concluding remarks

We acknowledge that the glial-canal-hypothesis presented here contradicts current understanding of structure in neuroscience. We have thus provided numerous picture panels to support our

statements. We have countless additional supportive experiments, images and data that are too extensive to include into one manuscript. We are happy to provide access to our preparations, technology, data and images to the neuroscience community and strongly encourage the independent re-investigation of cellular structure in the human and mammalian nervous system by other investigators. We suggest that particular focus should be given to the identity of myelinated cell profiles using ultrastructural serial section analysis to unambiguously demonstrate the origin of myelinated cell processes in the brain.

ACKNOWLEDGEMENTS

The authors would like to thank Melanie Winters and Shane Grandusky for assistance with the uptake experiments. We thank Dr. John DeWitt for support and access to human decedent tissue. We thank Drs. Alain Brizard, Christopher Francklyn, Mark Nelson, Mark Lubkowitz, Douglas Taatjes, and Heather Driscoll for support and helpful feedback on this work. We thank Ann and Dr. David MacLaughlin for their donation to fund the Zeiss confocal microscope. The Electron Microscopic investigations were performed at the Microscopy Imaging Center at the University of Vermont (RRID: SCR_018821). We thank Natalie Cashen, Dr. Gerald Herrera, Nicole Bouffard, Kyra Lee, and Brad Vietje for technical support. Research reported in this publication was supported by an Institutional Development Award (IDeA) from the National Institute of General Medical Sciences of the National Institutes of Health under grant number P20GM103449. Its contents are solely the responsibility of the authors and do not necessarily represent the official views of NIGMS or NIH.

Conflict of Interest:

Dr. Adam Weaver and Abigail Roman declare no competing financial interests.

Saint Michael's College together with Dr. Ruth Fabian-Fine have filed a patent as a direct result of this research.

AUTHOR CONTRIBUTIONS

Conceptualization: RFF

Funding acquisition: RFF, ALW

Methodology: RFF

Project administration: RFF

Supervision: RFF

Investigation: RFF, ALW, AGR

Visualization: RFF, AGR, ALW

Formal Analysis: ALW

Resources: RFF, ALW

Validation: RFF

Writing – original draft: RFF

Writing – review & editing: RFF, ALW

RESOURCE AVAILABILITY

Lead contact:

Further information and requests for the resources and reagents should be directed to and will be fulfilled by the lead contact, Dr. Ruth Fabian-Fine (rfabianfine@smcvt.edu).

Materials availability:

In the context of this study, no new unique reagents were created.

Data and code availability:

- All data reported in the main text and/or the supplementary materials of this paper will be shared by the lead contact upon reasonable request.
- This paper does not report original code.
- Any additional information required to reanalyze the data reported in this paper is available from the lead contact.

REFERENCES

Abbott, N.J., Pizzo, M.E., Preston, J.E., Janigro, D., Thorne, R.G., 2018. The role of brain barriers in fluid movement in the CNS: is there a 'glymphatic' system? Acta neuropathologica. 135, 387-407.

Agre, P., King, L.S., Yasui, M., Guggino, W.B., Ottersen, O.P., Fujiyoshi, Y., Engel, A., Nielsen, S., 2002. Aquaporin water channels – from atomic structure to clinical medicine. Journal of Physiology. 542, 3-16.

Alonso, R., Pisa, D., Marina, A.I., Morato, E., Rábano, A., Rodal, I., Carrasco, L., 2015. Evidence for fungal infection in cerebrospinal fluid and brain tissue from patients with amyotrophic lateral sclerosis. International Journal of Biological Sciences. 11, 546.

Amiry-Moghaddam, M., Ottersen, O.P., 2003. The molecular basis of water transport in the brain. Nature Reviews Neuroscience. 4, 991-1001.

Badaut, J., Fukuda, A.M., Jullienne, A., Petry, K.G., 2014. Aquaporin and brain diseases. Biochim Biophys Acta. 1840, 1554-65.

Barichello de Quevedo, J.L., Leffa, D.T., Pascoal, T.A., 2023. Glymphatic system waste clearance and Alzheimer's disease. Braz J Psychiatry. 45, 385-386.

Bruno, F., Abondio, P., Bruno, R., Ceraudo, L., Paparazzo, E., Citrigno, L., Luiselli, D., Bruni, A.C., Passarino, G., Colao, R., Maletta, R., Montesanto, A., 2023. Alzheimer's disease as a viral disease: Revisiting the infectious hypothesis. Ageing Research Reviews. 91.

Buccellato, F.R., D'Anca, M., Serpente, M., Arighi, A., Galimberti, D., 2022. The Role of Glymphatic System in Alzheimer's and Parkinson's Disease Pathogenesis. Biomedicines. 10.

Fabian-Fine, R., Aiken, A.M., Aug, J.R., Boucher, J.D., Butler, D.C., Clancy, L.J., Clem, S.A., Crotty, S.C., Dalpe, A.M., Donzello-Jewett, E.J., Galgay, T.M., Gillis, B.K., Heinrich, B.W., Hines, K.R., Kimmel, J.E., McGrath, J.M., Miles, M.M., Morey, J.A., Ortiz, I.A., Pham, K.Q., Quinn, L.C., Radican, C.J., Speidel, N.T., Thomas, B.J., Troisi, A.R., Weiss, J.L., Wentzheimer, K.V., Weaver, A.L., 2023. Neurodegeneration in a novel invertebrate model system: Failed microtubule-mediated cell adhesion and unraveling of macroglia. Journal of Comparative Neurology. 531, 618-638.

Fabian-Fine, R., Weaver, A.L., Roman, A.G., Winters, M.J., DeWitt, J.C., 2024. Myelinated Glial Cells: Their Proposed Role in Waste Clearance and Neurodegeneration in Arachnid and Human Brain. J Comp Neurol. 532, e70000.

Forrest, S.L., Kim, J.H., Crockford, D.R., Huynh, K., Cheong, R., Knott, S., Kane, M.A., Ittner, L.M., Halliday, G.M., Kril, J.J., 2023. Distribution Patterns of Astrocyte Populations in the Human Cortex. Neurochem Res. 48, 1222-1232.

Garman, R.H., 2011. Histology of the central nervous system. Toxicol Pathol. 39, 22-35.

Gupta, A., Goyal, R., 2016. Amyloid beta plaque: a culprit for neurodegeneration. Acta Neurol Belg. 116, 445-450.

Iliff, J.J., Wang, M., Liao, Y., Plogg, B.A., Peng, W., Gundersen, G.A., Benveniste, H., Vates, G.E., Deane, R., Goldman, S.A., Nagelhus, E.A., Nedergaard, M., 2012. A paravascular pathway facilitates CSF flow through the brain parenchyma and the clearance of interstitial solutes, including amyloid β. Science Translational Medicine. 4, 147ra111.

Iliff, J.J., Nedergaard, M., 2013. Is there a cerebral lymphatic system? Stroke. 44, S93-S95.

Jo, A.O., Ryskamp, D.A., Phuong, T.T., Verkman, A.S., Yarishkin, O., MacAulay, N., Krizaj, D., 2015. TRPV4 and AQP4 Channels Synergistically Regulate Cell Volume and Calcium Homeostasis in Retinal Muller Glia. J Neurosci. 35, 13525-37.

Komori, T., 2017. Pathology of oligodendroglia: An overview. Neuropathology. 37, 465-474.

Liedtke, W., Friedman, J.M., 2003. Abnormal osmotic regulation in trpv4-/- mice. Proc Natl Acad Sci U S A. 100, 13698-703.

Maarouf, C.L., Daugs, I.D., Spina, S., Vidal, R., Kokjohn, T.A., Patton, R.L., Kalback, W.M., Luehrs, D.C., Walker, D.G., Castano, E.M., Beach, T.G., Ghetti, B., Roher, A.E., 2008. Histopathological and molecular heterogeneity among individuals with dementia associated with Presenilin mutations. Mol Neurodegener. 3, 20.

Mancuso, R., Sicurella, M., Agostini, S., Marconi, P., Clerici, M., 2019. Herpes simplex virus type 1 and Alzheimer's disease: link and potential impact on treatment. Expert review of anti-infective therapy. 17, 715-731.

Mestre, H., Hablitz, L.M., Xavier, A.L.R., Feng, W., Zou, W., Pu, T., Monai, H., Murlidharan, G., Castellanos Rivera, R.M., Simon, M.J., Pike, M.M., Plá, V., Du, T., Kress, B.T., Wang, X., Plog, B.A., Thrane, A.S., Lundgaard, I., Abe, Y., Yasui, M., Thomas, J.H., Xiao, M., Hirase, H., Asokan, A., Iliff, J.J., Nedergaard, M., 2018. Aquaporin-4-dependent glymphatic solute transport in the rodent brain. eLife. 7, e40070.

Möbius, W., Cooper, B., Kaufmann, W.A., Imig, C., Ruhwedel, T., Snaidero, N., Saab, A.S., Varoqueaux, F., 2010. Electron microscopy of the mouse central nervous system. In Methods in cell biology. Vol. 96, ed.^eds. Elsevier, pp. 475-512.

Möbius, W., Nave, K.-A., Werner, H.B., 2016. Electron microscopy of myelin: Structure preservation by high-pressure freezing. Brain Research. 1641, 92-100.

Moore-Maxwell, C.A., Datto, M.B., Hulette, C.M., 2004. Chemotherapy-induced toxic leukoencephalopathy causes a wide range of symptoms: a series of four autopsies. Mod Pathol. 17, 241-7.

Murdock, M.H., Yang, C.Y., Sun, N., Pao, P.C., Blanco-Duque, C., Kahn, M.C., Kim, T., Lavoie, N.S., Victor, M.B., Islam, M.R., Galiana, F., Leary, N., Wang, S., Bubnys, A., Ma, E., Akay, L.A., Sneve, M., Qian, Y., Lai, C., McCarthy, M.M., Kopell, N., Kellis, M., Piatkevich, K.D., Boyden, E.S., Tsai, L.H., 2024. Multisensory gamma stimulation promotes glymphatic clearance of amyloid. Nature. 627, 149-156.

Nahirney, P.C., Tremblay, M.-E., 2021. Brain ultrastructure: putting the pieces together. Frontiers in cell and developmental biology. 9, 629503.

Nedergaard, M., 2013. Neuroscience. Garbage truck of the brain. Science. 340, 1529-1530.

Nedergaard, M., Goldman, S.A., 2016. Brain Drain. Scientific American. 314, 44-49.

Niu, H., Alvarez-Alvarez, I., Guillen-Grima, F., Aguinaga-Ontoso, I., 2017. Prevalence and incidence of Alzheimer's disease in Europe: A meta-analysis. Neurologia. 32, 523-532.

Preston, G.M., Carroll, T.P., Guggino, W.B., Agre, P., 1992. Appearance of Water Channels in Xenopus Oocytes Expressing Red Cell CHIP28 Protein. Science. 256, 385-387.

Sait, A., Angeli, C., Doig, A.J., Day, P.J.R., 2021. Viral Involvement in Alzheimer's Disease. ACS chemical neuroscience. 12, 1049-1060.

Sigurdson, C.J., Bartz, J.C., Glatzel, M., 2019. Cellular and Molecular Mechanisms of Prion Disease. Annual review of pathology. 14, 497-516.

Smith, T.W., Anwer, U., DeGirolami, U., Drachman, D.A., 1987. Vacuolar change in Alzheimer's disease. Arch Neurol. 44, 1225-8.

Stirling, D.R., Swain-Bowden, M.J., Lucas, A.M., Carpenter, A.E., Cimini, B.A., Goodman, A., 2021. CellProfiler 4: improvements in speed, utility and usability. BMC Bioinformatics. 22, 433.

Trejo-Lopez, J.A., Yachnis, A.T., Prokop, S., 2022. Neuropathology of Alzheimer's Disease. Neurotherapeutics. 19, 173-185.

Tycko, R., 2015. Amyloid polymorphism: structural basis and neurobiological relevance. Neuron. 86, 632-45.

Wang, S., Solenov, E.I., Yang, B., 2023. Aquaporin inhibitors. In Aquaporins. Vol., ed.^eds. Springer, pp. 317-330.

Whatley, B.R., Li, L., Chin, L.S., 2008. The ubiquitin-proteasome system in spongiform degenerative disorders. Biochim Biophys Acta. 1782, 700-12.

1 **FIGURE LEGENDS**

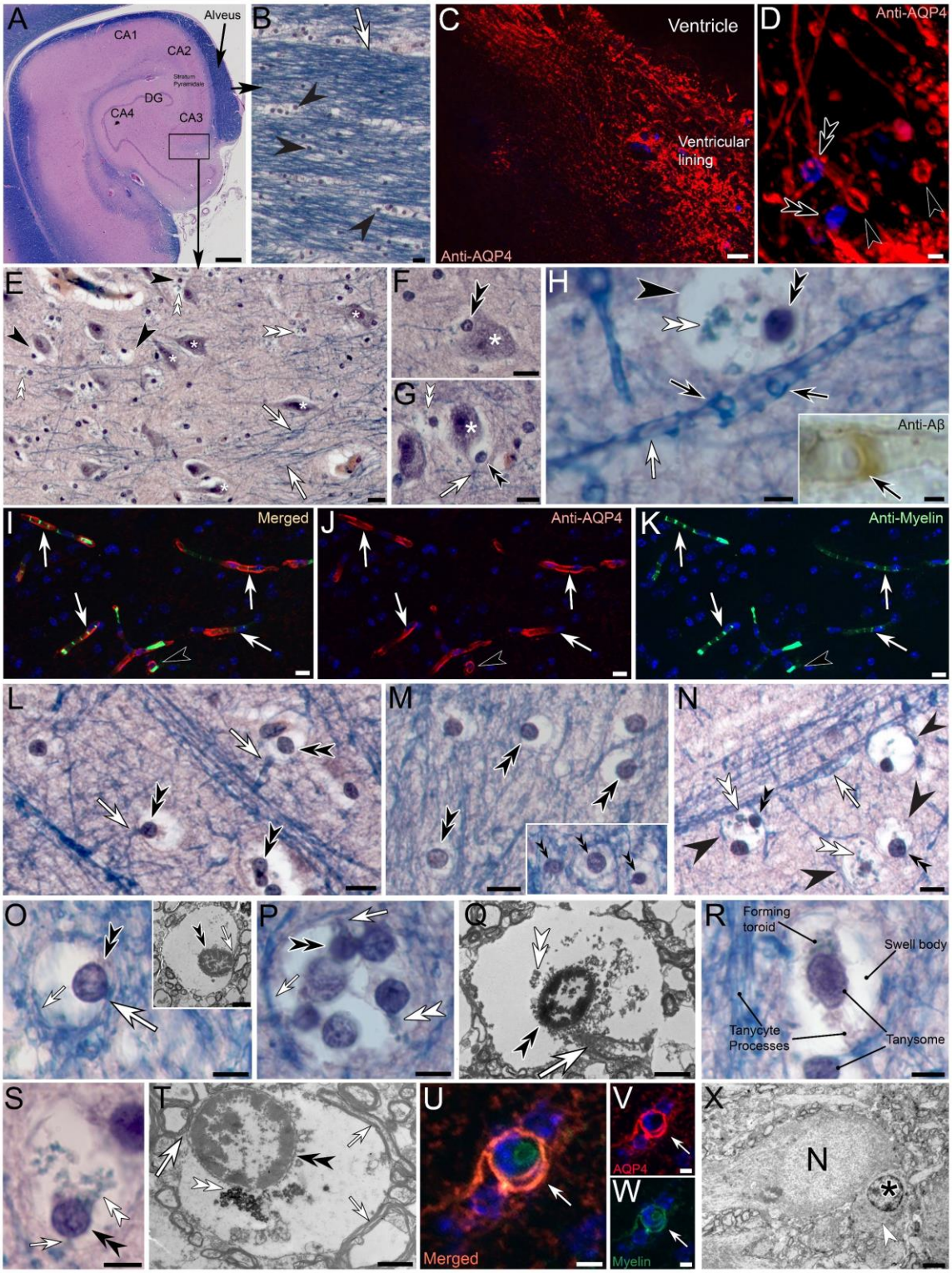

2

Figure 1. Myelinated Ependymal tanycytes in human and mouse hippocampus project into the hippocampal stratum pyramidale and give rise to waste-internalizing receptacles. (A-B) The alveus of human hippocampus contains numerous Luxol H&E-stained ependymal tanycytes that send vast numbers of slender myelinated processes (*white arrow in B*) into the stratum pyramidale of the hippocampal formation. Numerous electron-lucent 'swell-bodies' with associated nucleus-like tanysomes are forming along individual myelinated processes (*black arrowheads in B*). **(C, D)** Aquaporin4-immunolabeling of human alveus shows strong immunoreactivity of tanycyte processes. Higher magnification *(D)* shows Hoechst-blue stained nucleus-like structures in close association with tanycytes (*black double arrowheads in D*). Circular, immunoreactive swellings can be observed along the tanycyte processes (*black arrowheads*). **(E-G)** Luxol-blue stained human tanycyte processes (white arrows) project into the stratum pyramidale where they form translucent swell-bodies (black arrowheads) with associated nucleus like tanysomes (*black double arrowheads*). Please note the close association of swell-bodies with neuronal somata (*asterisks*). **(H)** Tanycyte (*white arrow*) with associated translucent swell body (*black arrowhead*) with tanysome (*black double arrowhead*) with emanating waste receptacles (*white double arrowhead*). Swelling ring structures (*black arrows*) that line the inside of swelling tanycyte processes are visible in Luxol H&E-stained and Aβ-immunolabeled (*black arrow in inset*) tanycyte processes. **(I-K)** AQP4 (*red*) and myelin (*green*) immunolabeling of mouse hippocampus shows double labeled tanycyte processes that contain myelin-immunoreactive circular profiles that line the inner lumina of the cell processes (*white arrows*). *Black arrowhead:* AQP4-immunolabled swell body. **(L-N)** Tanycyte processes (*white arrows*) with associated swell-bodies (*black arrowheads*) in human stratum pyramidale. *White double arrowheads:* forming receptacles; *Black double arrowheads:* Tanysomes. *Inset in M*: Forming tanysomes in the alveus. **(O-T)** Structural characteristics of swell bodies, associated tanysomes (*black double arrowheads*) and receptacles (*white double arrowheads*) in human hippocampus. Both light and ultrastructural images show the electron lucent nature of the swell bodies. Each swell body contains between one and 6 tanysomes that are stained for nuclear stain in Luxol H&E-stained preparations and appear associated with myelinated tanycyte processes (*white arrows*). Tanysomes give rise to toroids and receptacles some of which

appear electron-dense at the ultrastructural level (*white double arrowheads in T*). Please note the myelinated tanycyte profiles that line the circumference of swell bodies (*small white arrows in O, P, T*). **(U-W)** AQP4/Myelin immunolabeled swell body in mouse hippocampus shows the double-labeled nature of myelinated AQP4-immunoreactive tanycyte profiles (*white arrow*) around the periphery of swell bodies. **(X)** Typical structured appearance of a glial nucleus (*asterisk)* and surrounding cytoplasm (*white arrowhead*). **Scale bars:** A: 500 µm, B:10 µm, C: 20 µm; D: 5 µm; E-G: 10 µm, H: 5 µm, Inset 3 µm; I-N: 10 µm; M: 20 µm; N: 10 µm; O: 5 µm, (*Inset*) 2 µm; P: 5 µm Q 2 µm R: 5 µm; S: 5 µm; T: 2 µm; U-W: 5 µm; X: 2 µm.

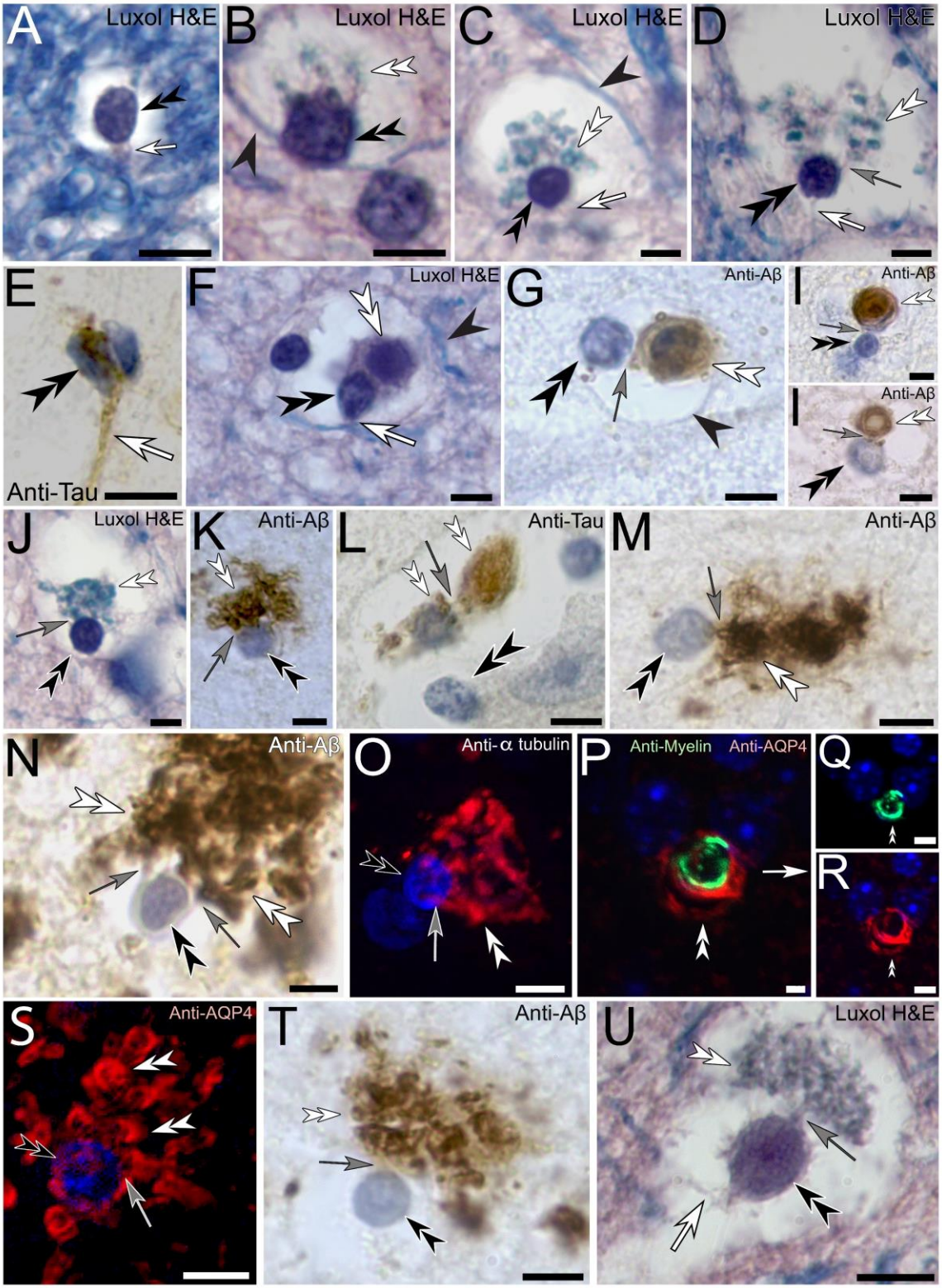

Figure 2. Tanysomes in human and mouse hippocampus give rise to toroids and receptacles that are immunoreactive for Aβ, hyperphosphorylated tau protein, myelin, AQP4 and α-

tubulin. (A-O) Human hippocampal tanysomes within swell-bodies give rise to a network of membranous receptacles and toroids (*white double arrowheads*). The physical attachment between tanysomes (*black double arrowheads*) and tanycyte processes (*white arrows*) and receptacles (*grey arrows*) is clearly visible. Nuclear stain is observed in both tanysomes and emanating toroid-shaped ring structures (*F, G, H*). The tanysome-derived membrane network in human brain is immunoreactive for tau-protein (*E, L*), Aβ (G, *H, I, K, M, N*) and α-tubulin (*O)*. **(P-R)** Immunolabeling of mouse hippocampus for anti-AQP4 (*red*) and myelin (*green*) demonstrates that toroids that emerge from tanysomes are immunoreactive for both epitopes. **(S-U)** Tanysome-derived receptacles in preparations immunolabeled for anti-AQP4 (S), anti-Aβ (T) and stained for Luxol H&E (U) consistently demonstrate their physical association with tanysomes (*grey arrows*). Scale bars: A-U: 5 μm.

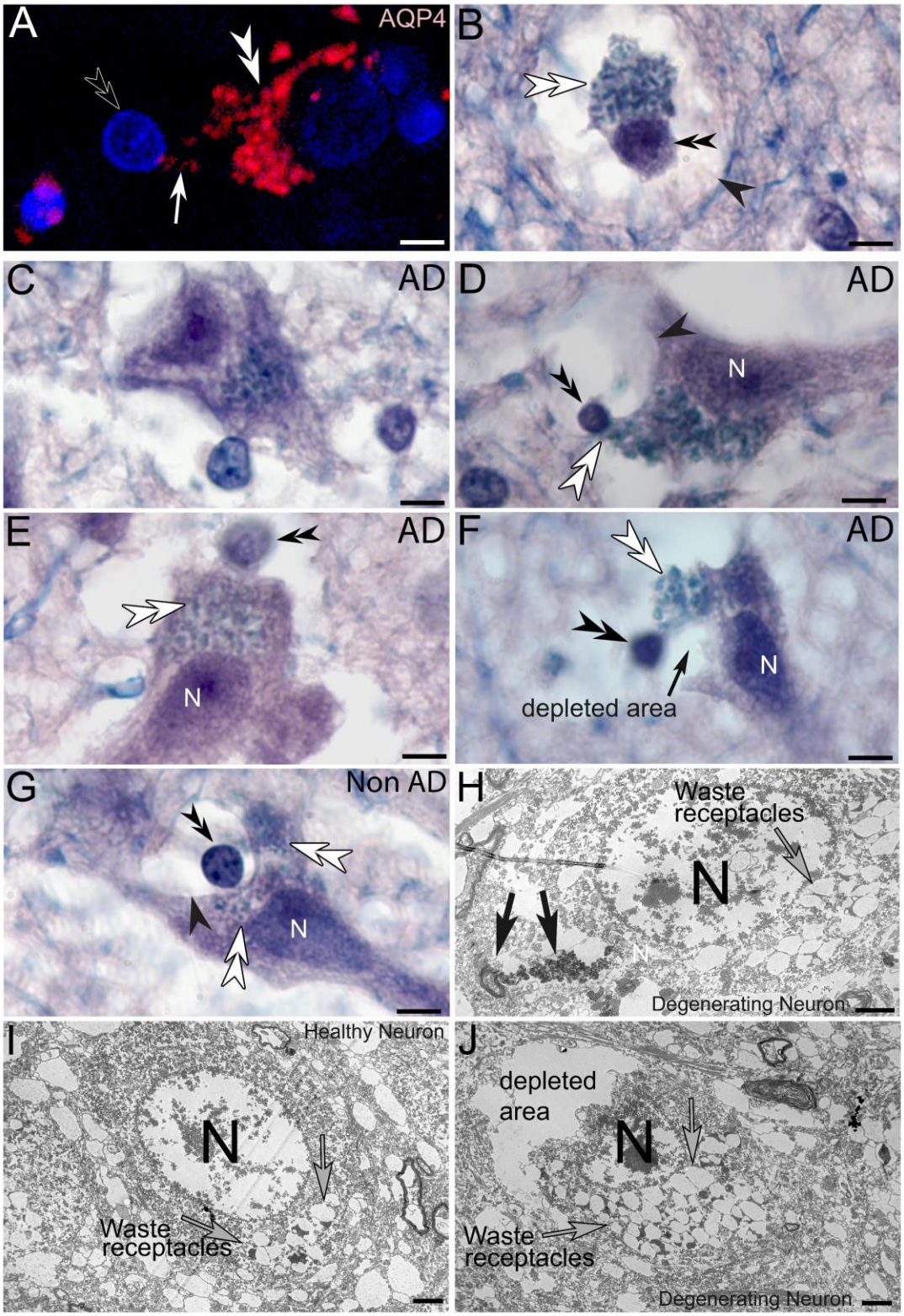

Figure 3. Tanysome-derived waste receptacles in human hippocampus project into neuronal somata. (A) Tanysome-derived (*black double arrow*) waste receptacles are immuno-positive for

aquaporin-4 (*white double arrowhead*). **(B-G)** Luxol H&E-stained preparations show the characteristically blue stained tanysome-derived waste receptacles that differentiate in swell-bodies (*panel B*) project into pyramidal cell somata. *Black double arrowhead*s: Tanysomes; *White double arrowhead*s: Waste receptacles; *Black arrowheads*: Outer margins of swell-bodies; *N*: Neuronal somata. **(H-J)** Ultrastructural depiction of healthy and degenerating neuronal somata demonstrates the abundance of swelling waste receptacles and gradual depletion of cytoplasmic areas in degenerating somata (*H, J*) compared to the much sparser number of waste receptacles in a healthy neuron that shows an intact cytoplasmic structure (*I*). Please note the waste accumulation associated with a waste receptacle strand that emanates from a myelinated cell profile (arrows in H) consistent with strands of waste receptacles observed at the light microscopic level (C-G). Scale bars: A-G: 5 µm; H-J: 2 µm.

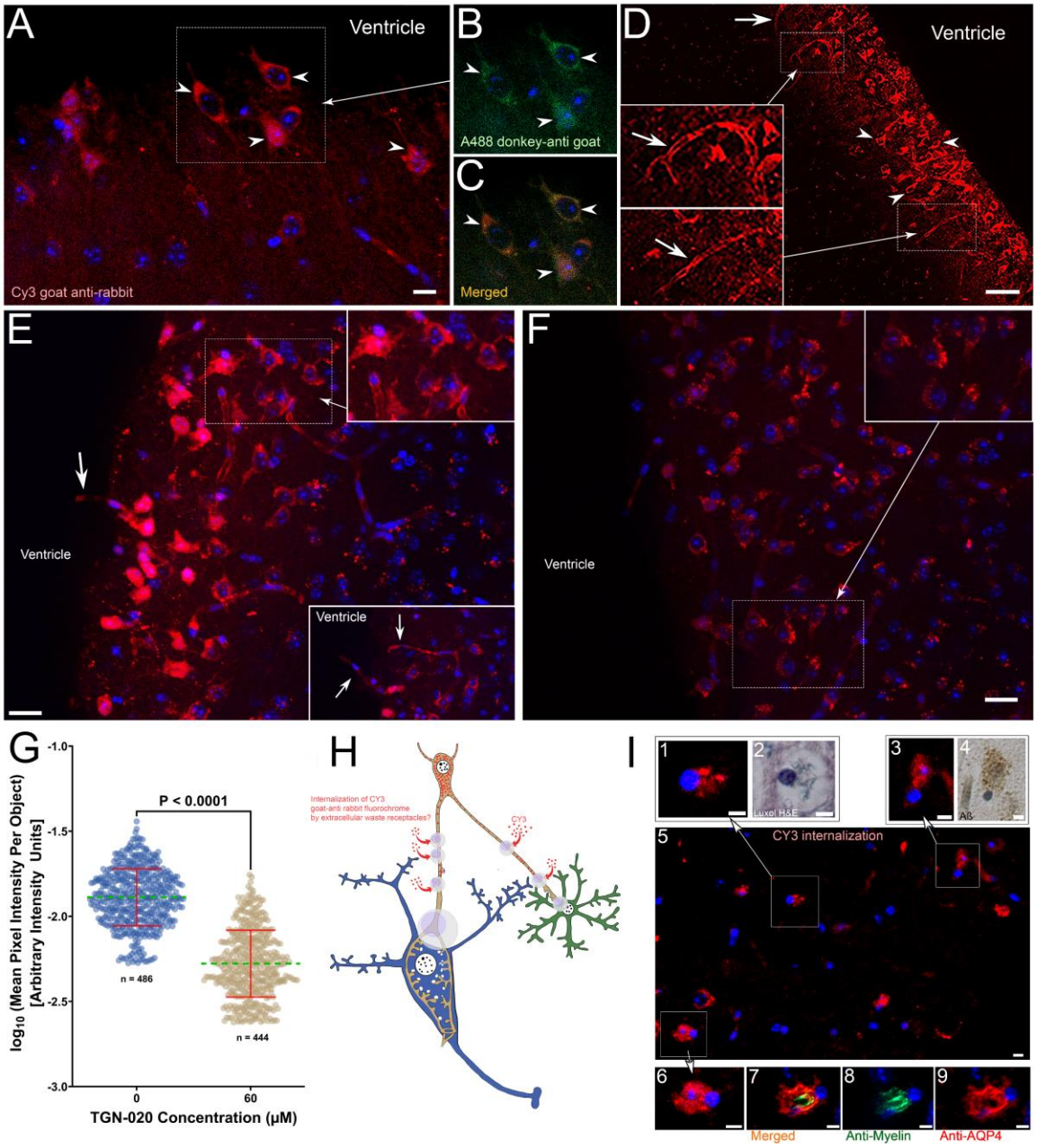

Figure 4. Evidence for aquaporin-4-dependent Cy3 goat anti-rabbit antibody internalization into living mouse hippocampal ependymal tanycytes. (A-C) Living ependymal tanycytes that were exposed to Cy3 goat anti rabbit antibody appear fluorescent after 30 min exposure (*white arrowheads in A*). Immunolabeling against goat-protein using an Alexa 488-coupled donkey-anti-goat antibody demonstrates co-localization of both Cy3 and Alexa 488 fluorochromes (*white arrowheads in B, C*) indicative that the red fluorescence within tanycytes originates from internalized Cy3 goat anti rabbit antibody. **(D)** Ependymal tanycytes in mouse alveus show red

fluorescence after 30 min exposure of living brain tissue to Cy3 goat anti-rabbit antibody (*white arrowheads*). A fine network of fluorescing processes (*grey arrowhead*) is visible in the stratum pyramidale. *Insets:* Canal structures each containing two fluorescing channels (arrows) are frequently observed projecting into the adjacent ventricle. **(E, F)** Normalized intensity of internalized Cy3 fluorochrome comparing control (0; *E*) and AQP4-blocked (60 μM TGN-020; *F*) conditions. Control cells demonstrate a higher pixel intensity, especially towards the alveus. **(G)** Log_{10} mean cellular object intensity is significantly larger in control (0 μM; -1.888) compared to AQP4-blocked (60 μM TGN-020; -2.278; $t(928) = 32.666$, $p = 2.44 \times 10^{-156}$, unpaired two-tailed *t*-test). Inset in E: Fluorescent canal structures extending into the ventricle (white arrows). **(H)** Schematic depiction of the proposed waste internalization demonstrated here. We postulate that living tanycytes internalize surrounding fluorochromes via extracellular waste receptacles that are formed within swell-bodies explaining the observed fluorescence in ependymal tanycytes. To visualize cells, Hoechst blue nuclear stain was applied after fixation of the brains. **(I)** Single 3- μm optical confocal section of mouse brain with internalized fluorochromes. Note the strong resemblance of brightly fluorescent tanysome-like areas (*1, 3, 5, 6*) with toroid- and receptacle-forming human tanysomes (*2, 4*) and AQP4/myelin-doublelabeled mouse tanysomes (*7-9*). Scale bars: A-C: 10 μm, D: 50 μm; E, F: 20 μm; H: not drawn to scale; I: 5 μm.

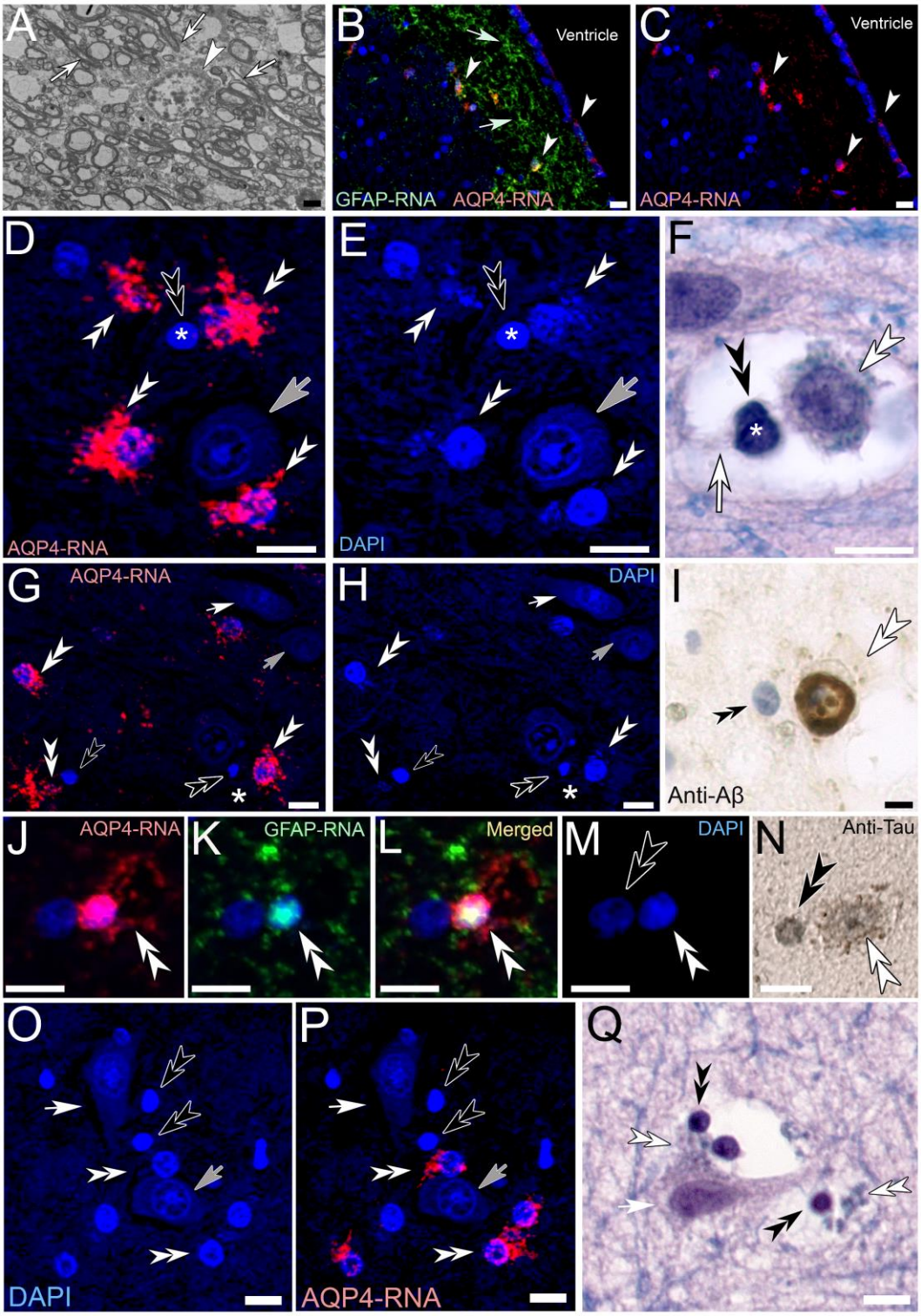

Figure 5: RNA-scope gene expression within tanycytes and associated swell-bodies of human hippocampus in both AD-affected and AD-unaffected tissue. (A) Electron micrograph of a tanycyte soma (*white arrowhead*) in the alveus of AD-affected tissue shows myelinated

tanycyte processes projecting from the soma (*white arrows*). **(B, C)** RNA-scope visualization of RNA expression for glial-fibrillary acid protein (GFAP; *green*) and aquaporin-4 (AQP4; *red*) demonstrate the expression of both RNAs in the alveus (white arrowheads). Please note the abundance of GFAP within tanycyte processes indicative of RNA-transport (green arrows). **(D, E)** AQP4-RNA expression in the stratum pyramidale counter-stained with DAPI nuclear stain shows brightly fluorescing tanysomes (*black double arrowheads*) with emerging waste receptacles (*white double arrowheads*). Please note the absence of staining in the astrocyte-like cell soma (*grey arrows*). **(F)** Luxol H&E stained tanysome (black arrowhead) with emerging receptacle-forming toroid (white double arrowhead) strongly resembles the AQP4-expressing tanysome indicated by the *asterisk in D, E*. **(G, H)** AQP4-expressing waste receptacles (*white double arrowheads*) that emerge from tanysomes (*black double arrowheads*). Cell somata resembling a neuron (*white arrow*) and adjacent astrocyte (*grey arrow*) are void of AQP4-RNA expression. **(I)** Tanysome (*black double arrowhead*) with emerging anti Aβ-stained toroid (*white double arrowheads*) strongly resembles the AQP4-RNA expressing tanysome indicated by the *asterisks in G, H*. **(J-M)** Receptacle-forming (*white double arrowheads*) tanysome (*black double arrowheads*) show co-expression for GFAP (*green, white double arrowheads*) and AQP4 (*red*). **(N)** Anti-tau-stained tanysome (*black double arrowhead*) with associated receptacle-forming toroid (*white double arrowheads*) strongly resemble the tanysome shown in *J-M*. **(O-P)** AQP4-RNA expression is restricted to receptacle-forming tanysomes (*white and black double arrowheads*) that are in close contact to an unstained neuronal soma (*white arrow*) and an unstained astrocyte-like soma (*grey arrow*). **(Q)** Luxol H&E-stained pyramidal cell soma (*white arrow*) shows the consistency of the RNA-scope labeling in *O, P* whereby receptacle forming tanysomes (*white and black double arrowheads*) are adjacent to neuronal soma. **Scale Bars:** A: 2 μm; B, C: 5 μm; D-H: 10 μm; I: 5 μm; J-Q: 10 μm.

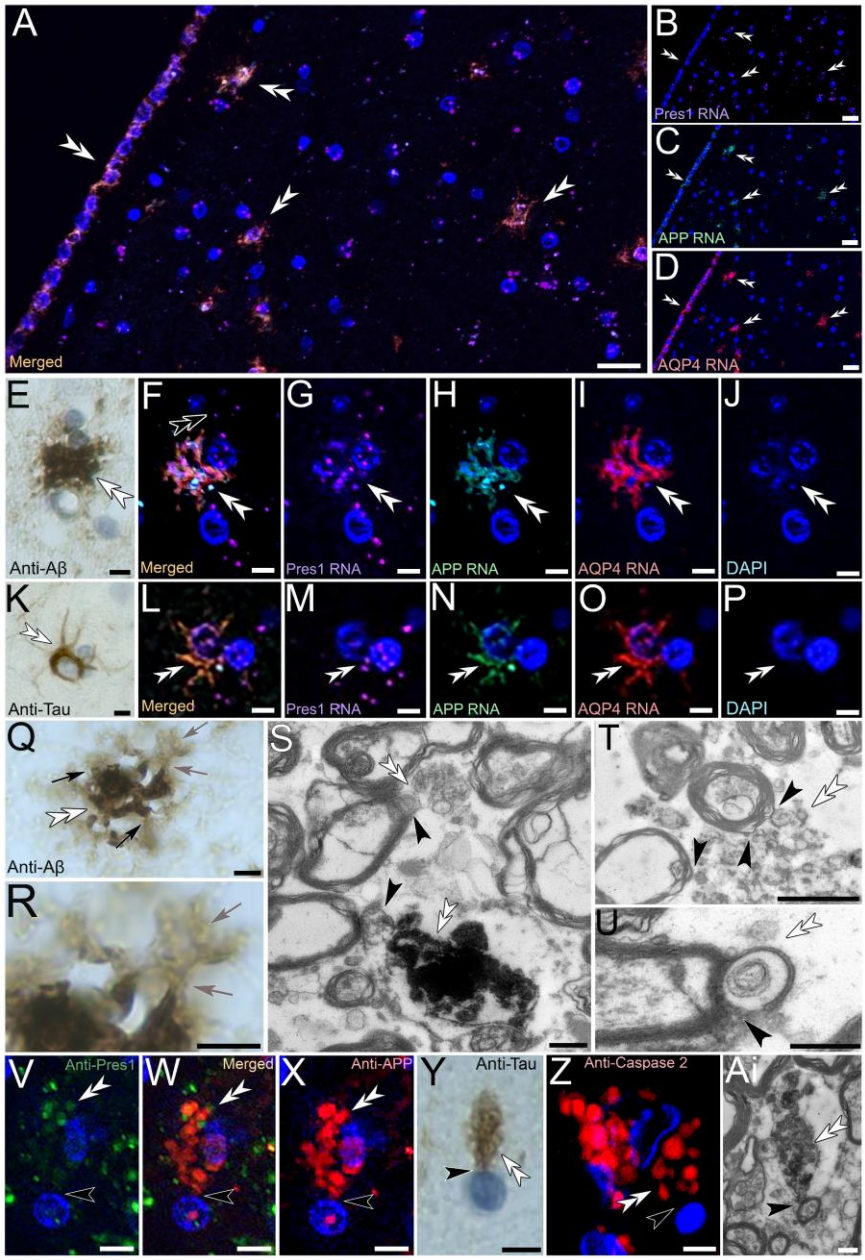

Figure 6. Amyloid β-related gene expression in Alzheimer Disease-affected human hippocampus. (A-D, F-J, L-P) Ependymal tanycytes in the ventricular lining show RNA-co-expression for Presenilin1 (*Pres-1*, *magenta*), Amyloid Precursor Protein (*APP*, *green*) and Aquaporin 4 (*AQP4*, *red*). Higher magnification (*F-J, L-P*) shows that gene expression is associated with tanysome-derived toroids and receptacles (*DAPI nuclear stain*). **(E)** Tanysome-associated waste receptacles are strongly Aβ-immunoreactive (*white double arrowheads*) consistent with observed Pres1 and APP gene expression shown in *F-J*. **(K)** Anti-tau immunoreactive tanysome-

associated toroid. **(Q, R)** Anti Aβ-immunoreactive toroid (white double arrowhead) with emerging waste receptacles (*black and grey arrows*). Grey arrows indicate the area shown at higher zoom in (*R)*. **(S-U)** Electron micrographs of forming waste receptacles (*white double arrowheads*) in swell-bodies that emerge from myelinated cell profiles (*black arrowheads*). (V-Ai) Tanysome-associated waste receptacles show immunolabeling for Pres1 (V, W), APP (W, X), Tau protein (Y) and Caspase 2 (Z). The appearance of the immunolabeled receptacles is consistent with the ultrastructural appearance of waste-containing receptacles (Ai). **Scale Bars:** A-D: 20 μm; E-R: 5 μm; S: T: U: 2 μm; V-Z: 5 μm; Ai: 500 nm.

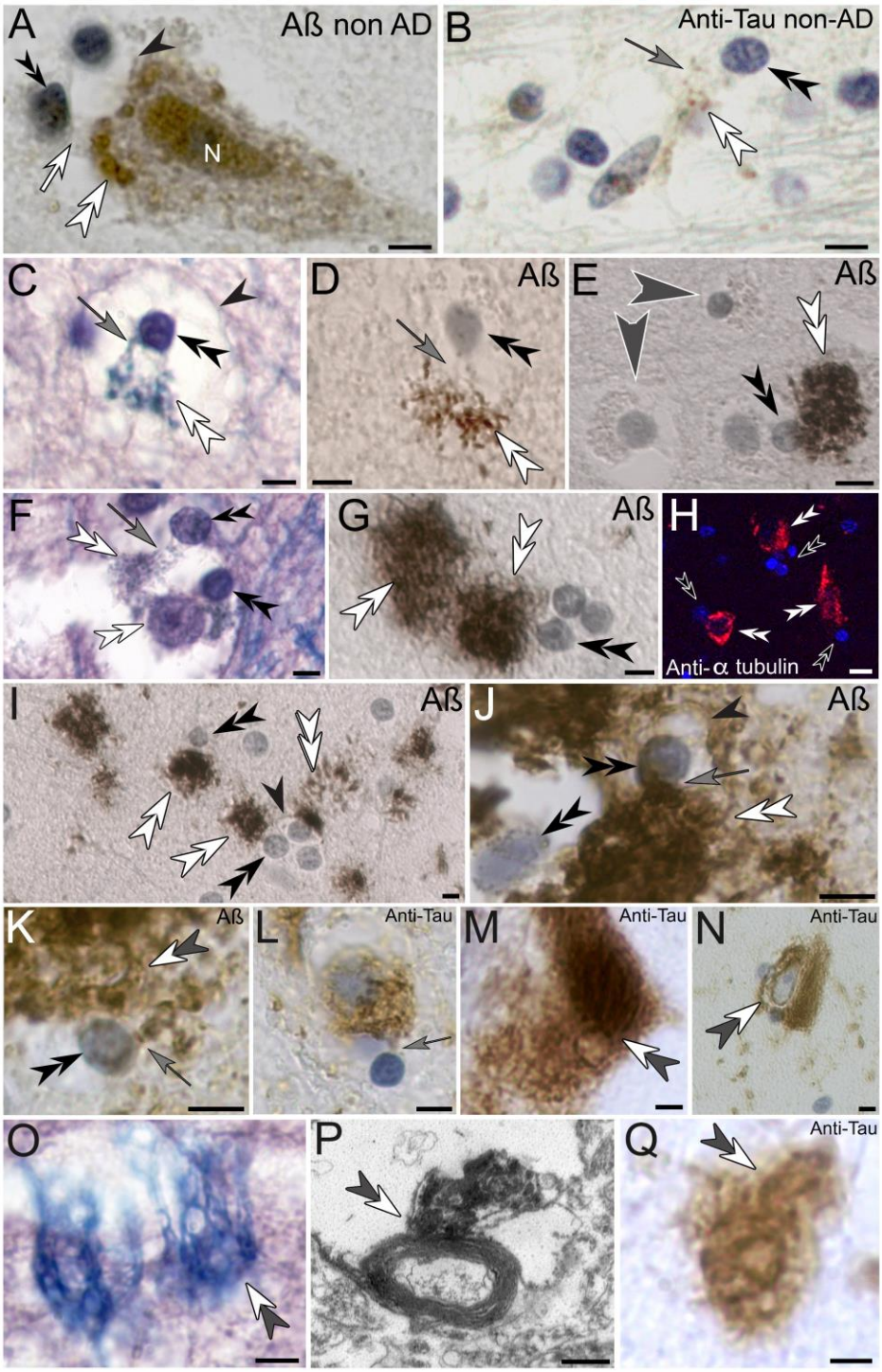

Figure 7. Tanysome-derived waste receptacles stain for Aβ, tau protein, and α-tubulin in AD-affected human brain tissue (A-B) Alzheimer Disease unaffected brain tissue shows moderate immunolabeling for Aβ and tau protein in association with intraneuronal (*A*) and extracellular (*B*) waste receptacles. Generally, the signal for Aβ is stronger compared to the observed anti-tau

immunolabeling. **(C-Q)** Comparison of Luxol H&E-stained tanysome-derived receptacles and unraveling Luxol blue-stained ring structures in AD-affected brain tissue (*C, F, O*) demonstrates their structural similarities to Aβ immunolabeled (*D, E, G, I, J, K*), Anti-tau immunoreactive (*L, M, N, Q*) and anti α-tubulin immunolabeled (*H*) preparations. Please note the similarities of unraveling myelin-derived cell profiles of varying sizes (*O*) with unraveling myelinated cell profiles at the ultrastructural level (*P*). These unraveling toroids are consistent with unraveling toroids observed in the anti-tau labeled preparations (*L, M, N, Q*) that have the characteristic appearance of 'tau tangles' (*grey-white double arrowheads*). *Black double arrowhead*s: Tanysomes; *White double arrowhead*s: Forming receptacles; *Black arrowheads*: outer margins of swell-bodies; *N*: Neuronal soma. Scale bars: A-O: 5 μm; P: 500 nm; Q: 3 μm.

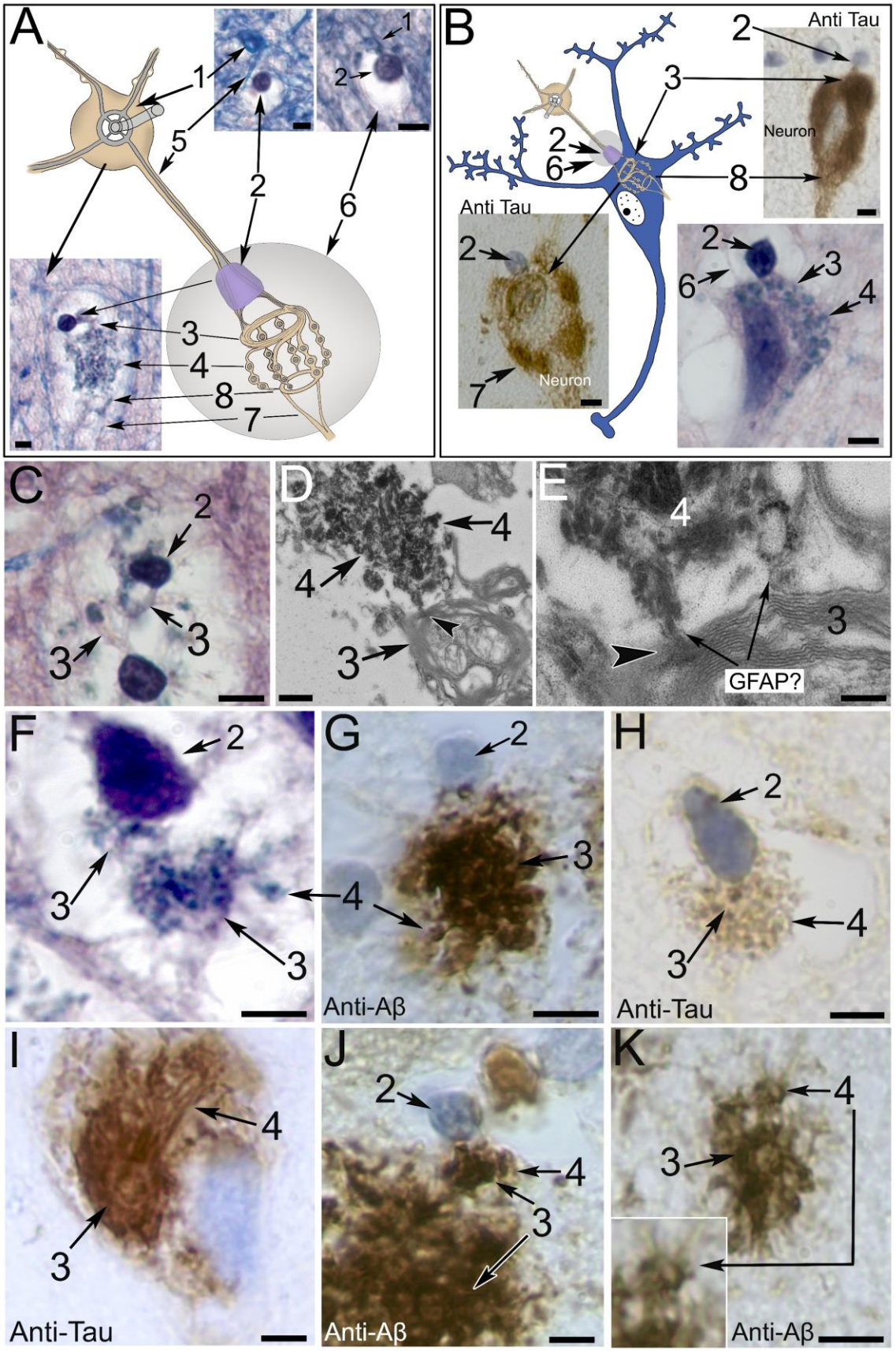
A
B
Anti Tau
Neuron
Anti Tau
Neuron
C
D
E
GFAP?
F
G
Anti-Aβ
H
Anti-Tau
I
Anti-Tau
J
Anti-Aβ
K
Anti-Aβ

1

Figure 8. Light- and electron-microscopic architecture of tanycyte-derived waste receptacles formed within swell bodies in the human brain. (A, B) Schematic depiction of the proposed structures that form within swell-bodies (*A*) and can be observed to project into neuronal somata (*B*). Swelling toroids (*1*) that are connected to an adjacent tanysome (*2*) via a slender tanycyte process (*5*). The tanysome gives rise to myelinated toroids (*3*) from which strands of waste-internalizing receptacles emerge (*4*). The individual receptacle strands terminate into a distal toroid-shaped ring structure (*8*) that merge into distal tanycyte processes (*7*). **(C-K)** The above-described structures and their proposed Luxol H&E-stained (C, F), anti-tau immunolabeled (*B, H, I*) and anti-Aβ immunolabeled (*G, J, K*) equivalents in AD-affected hippocampus are depicted and labelled accordingly within each panel. The tanysome-derived toroids and associated receptacle strands (*3, 4*) appear electron dense at the ultrastructural level and form large numbers of receptacles (*D, E*). The emerging tubular canal structures resemble glial fibrillary acid protein (*GFAP*, *black arrowhead in E*). Waste receptacles can be seen emanating from toroid-shaped ring structures in Luxol H&E-stained preparations (*white arrowhead in F*). Immunolabeling for Aβ shows similar immunolabeled waste receptacles (*G, J, K and inset*). Higher zoom shows the association of individual receptacles with a fine network of fibrillary canals consistent with the postulated stabilization of these proposed waste-internalizing structures by Aβ (*inset in K*). *6*: outer perimeter of swell body; Scale bars in light microscopic images: 5 µm; D: 500 nm; E: 150 nm. Schematic drawings not drawn to scale.

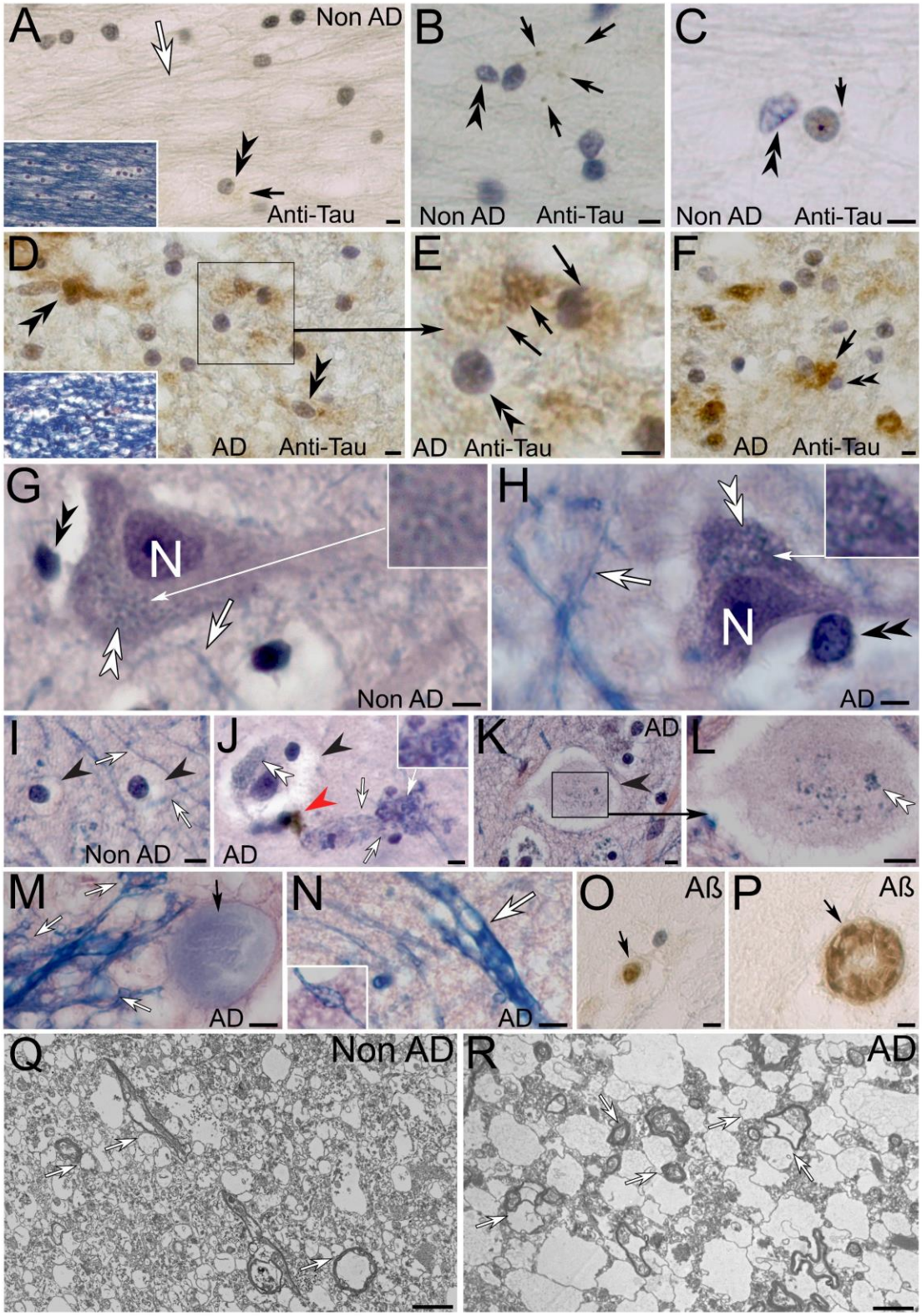

1

2 **Figure 9. Hypertrophic tanycyte swelling in human Alzheimer Disease (AD) affected brain**

3 **tissue. (A-C)** Tanycyte processes in the alveus (*white arrows*) in non-AD affected brain appear

linear and project parallel to each other in both anti-tau labeled brain tissue (*A*-*C*) and Luxol H&E-stained preparations (*inset in A*). Tanysome (*black double arrowheads*) derived waste receptacles are sparse and appear either unlabeled or weakly labeled for tau protein (*black arrows*). **(D-F)** The alveus in AD-affected brain tissue appears spongiform with bulging tanycyte processes in both anti-tau (*D*-*F*) and Luxol H&E-stained preparations (*inset in D*). Numerous swelling anti-tau labeled waste receptacles (black arrows) emanate from associated tanysomes (*back double arrowheads*). **(G, H)** Similar hypertrophic swelling can be observed in tanycyte processes (*white arrows in G compared to H*) and intraneuronal tanycyte receptacles (*white double arrowheads in G compared to H, higher zoom of receptacles in respective insets*). **(I-N)** Swell bodies and associated tanycyte profiles in non-AD affected tissue appear comparatively small and intact (*I*) compared to those in AD-affected brain tissue (*J*-*N*). In the latter swell bodies, tanysome-derived waste receptacles and associated tanycytes show abnormal hypertrophy (*J*-*L*). Please note the accumulation of brown deposit within the hypertrophic tanycyte process, indicative of a blockage by cellular waste (*red arrowhead in J*). Tanysomes and associated waste receptacles are difficult to recognize in swell-bodies that show advanced swelling stages (*K, L higher zoom that visualizes remaining waste receptacles*). Hypertrophic tanycyte processes form numerous swelling circular structures in comparison to those in non-AD affected tissue (*arrows in I compared to M, N, inset in N*). **(O, P)** Differences in swelling patterns are also observed in Aβ immunolabeled tanycyte-derived toroids (*arrows in O and P*). **(Q, R)** Comparison between non-AD (*Q*) and AD-affected tissue (*R*) at the ultrastructural level demonstrates abnormal spongiform swelling that originates from bulging myelin-derived tanycyte protrusions, (*white arrows in Q compared to R*). Scale bars: A-P: 5 μm, Q, R: 2 μm.

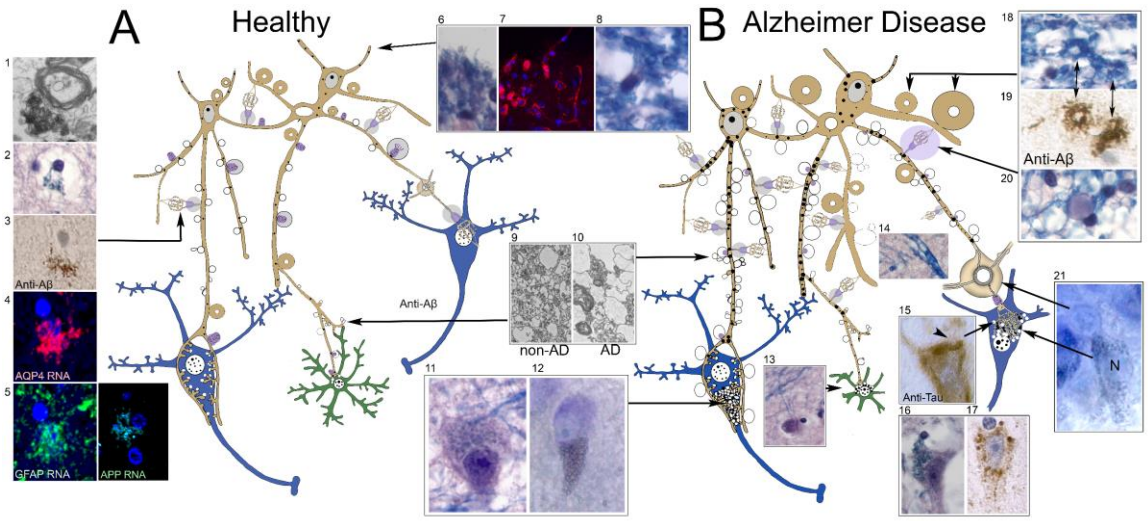

Figure 10. Schematic depiction of proposed tanycyte-derived waste canal system in the human hippocampus of healthy (A) and Alzheimer Disease (AD) affected brain tissue. (A) Neurons (*blue*) and glial cells (*green*) are contacted by myelinated aquaporin-4-expressing ependymal tanycytes (*beige*). The latter form both swelling toroids and waste receptacles (*1-5*) either directly from tanycyte protrusions (Fabian-Fine et al. 2024) or swell-body-derived that internalize and remove cellular waste from the brain parenchyma likely via apical drainage canals (*6-8*) in a proposed AQP4-dependent manner. We propose that receptacle formation is likely dependent on: (*i*) Amyloid β-mediated stabilization to prevent the collapse of waste-internalizing receptacles during this process, and (*ii*) tau-protein for the gradual and time appropriate release of waste receptacles. **(B)** In AD-affected brain tissue, hypertrophic tanycyte abnormalities that may be caused by physical waste obstruction lead to swelling of the tanycytes affecting the brain parenchyma (*9, 10*), intracellular waste receptacles that lead to dense obstruction of affected neurons and glial cells (*11, 12, 13*), tanycyte processes (*14*), and intraneuronal tanysome-derived receptacles (*15, 16, 17*). Swelling of tanycytes in the alveus leads to excessive sprouting of tanycyte-derived waste receptacles that appear Aβ immunoreactive (*18, 19*). Similar swelling can be observed in tanycyte-associated swell-bodies (*20*) and toroids (*21*). Schematics are not drawn to scale.

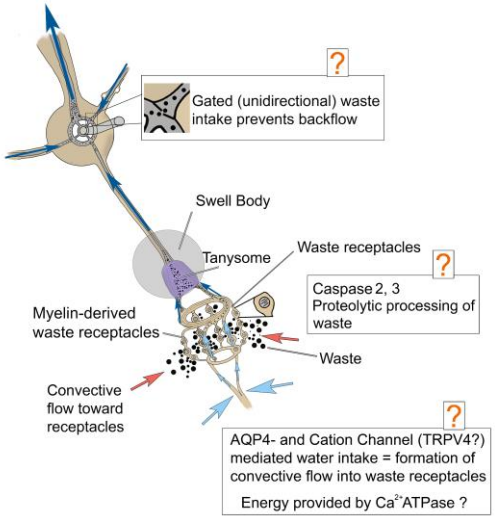

Figure 11. Proposed AQP4-mediated uptake mechanism of cellular waste into tanysome-derived waste receptacles. Swell-bodies differentiate myelin-derived AQP4-expressing receptacles that create a convective cytoplasmic flow toward the receptacles (light blue arrows) that flushes cellular debris particles toward the receptacles (red arrows). We postulate that receptacle-associated enzymes (e.g., Caspase 2) catabolize the debris prior to uptake into tanycytes. We propose that water influx into tanycytes may be calcium-mediated through the synergistic activation of TRPV4 cation channels. We postulate that swelling toroids that are formed along tanycytes may draw waste from the receptacles toward the toroids (dark blue arrows). We postulate that these canals may contain membrane-gated valves that prevent backflow. Schematic not drawn to scale.